Chapter 6: Spatiotemporal Self-Organization on a Partially Insulated Pt Ring Electrode

6.1 Introduction

On a ring electrode without insulator, studied in the chapter 3, all locations are equivalent by symmetry, the dominant patterns were standing waves and travelling pulses in the oscillatory state for close reference electrode (negative coupling favors the formation of inhomogeneous potential distributions). Travelling pulse occasionally reverses its direction spontaneously giving rise to spatiotemporal mixed-mode oscillations (SMMOs) [21]. If an electrode exhibits edges, *e.g.*, ribbon electrode in chapter 5, the situation is more complicated. The local effective resistance depends on position, and brings about local inhomogeneity, which means the electrode has different dynamic regimes. The strength, with which two points of the electrode couple together through migration, does not decay monotonically along the electrode, but the strength increases again towards the edge of the insulating plane where migration coupling diverges. For close reference electrode, the dominant patterns were anti-phase edge oscillations on a ribbon electrode [21].

In this chapter direct and isolated observations of edge effects by comparison of a ring with and without insulator are described. Figure 6.1 shows the assumption of the local $h(x)$ and coupling function $H(x, x')$ for the ring electrode with insulator (These have not been calculated ab initio from potential theory, but rather constructed piece-wise from earlier exact results for the ribbon and ring electrodes [34]). The local function remains constant over the most of the ring, but increases near the insulator because of the low effective resistance at the edges. As with the uninterrupted ring, the

coupling function $H(x, x')$ falls off with distance and becomes negative. It diverges at the edges, to $+\infty$ or $-\infty$ depending on the distance of the edges to the reference point x.

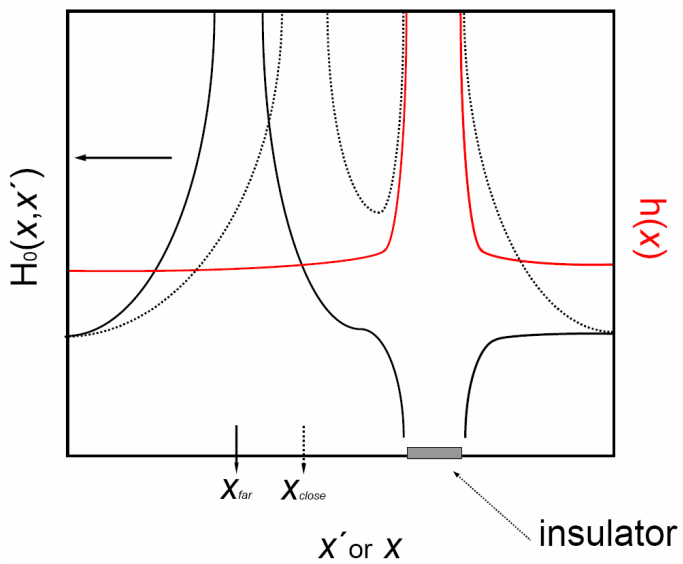

Figure 6.1. Schematic form of local $h(x)$ and coupling function $H_0(x, x')$ of ring electrode with insulator. $H_0(x, x')$ diverges at the edges to $+\infty$ or $-\infty$ when x is close to (far from) the edges.

An important motivation to study the influence of insulated areas on pattern formation (in particular travelling waves) comes from neurophysiology. Travelling excitation pulses (action potential) along unmyelinated axons can be well described by a continuous reaction-diffusion system (Hodgkin-Huxley theory) [28] though physically the coupling is mediated by field effects, and the propagation of an action potential along an unmyelinated axon is fundamentally the same as in a large number of continuous excitable media, from the Belousov-Zhabotinsky (BZ) reaction [102-105] to electrochemical pulses [3, 30, 101]. However, the presence of myelin changes the mode of transmission of the action potential. The action potential is unable to progress along the region of axon covered by insulating myelin. Thus, instead of smoothly invading each successive patch of membrane, action potentials jump from one node of Ranvier (uncovered membrane) to the next in myelinated axons (*saltatory conduction*). Compared to an unmyelinated axon the effective pulse velocity can be increased by up to 2 orders of magnitude.

6.2 Experimental

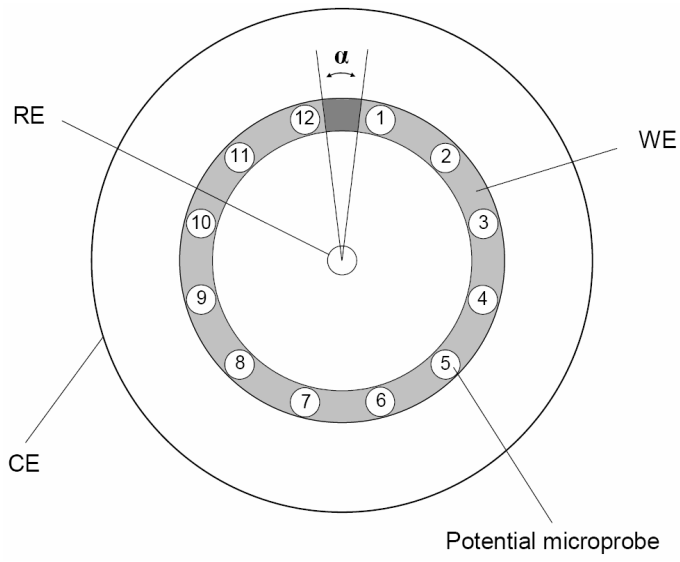

Figure 6.2. Schematic view of the electrode setup. Reference electrode is placed in the same plane as ring electrode. Ring electrode is coated by Apiezon wax (insulator) over an angled α between positions 1 and 12. Potential microprobes are separated by 30° angles, so α could be increased up to 30° without changing the setup.

A schematic view of the experimental setup is shown in Figure 6.2. A Pt ring of 34 mm inner and 40 mm outer diameter was used as a working electrode, which has locally an insulation part over an angle α (Apiezon wax) between positions 1 and 12; usually 5° insulator was used. A concentric platinized Pt wire ring used as counter electrode was placed 80 mm above the working electrode. The tip of a Luggin-Haber capillary hosting a Hg/Hg_2SO_4, K_2SO_4 (sat'd) reference electrode was placed at the center of the ring working electrode. The position of reference electrode is defined by the distance parameter β (β is the distance between the working electrode and the reference electrode divided by the outer radius of the working electrode). To detect the instantaneous local interfacial potentials on the Pt ring electrode, twelve microprobes were placed along the ring electrode close to the electrode surface (0.2 mm). Each microprobe capped with a Hg/Hg_2SO_4 electrode were filled a 0.5 M Na_2SO_4 solution (Merck, p.a.). All solutions were prepared with ultrapure water (Millipore Milli-Q water,

18 MΩ · cm) and were kept at room temperature. Before each experiment, the Pt ring electrode was chemically cleaned. For investigation of the electrocatalytic oxidation of formic acid, 0.1 M HCOONa (Merck, p.a.) in 0.033 M H_2SO_4 was used as the electrolyte. And we added 1×10^{-6} M bismuth ions into the main solution to reach oscillatory conditions. The electrolyte was extensively bubbled with N_2 before each experiment. A nitrogen atmosphere was maintained over the unstirred solutions during sweep experiments. Cyclic voltammetry and constant potential methods (effect of formic acid concentration by using reaction time; we also performed this method in chapter 3) were executed with a house built potentiostat (Electronic Laboratory of Fritz-Haber-Institut).

6.3 Experimental results

6.3.1 Pattern formation with close reference electrode ($\beta = 0$)

(A) Edge effect of insulator in the stationary states

We performed cyclic voltammetry with a non-insulated and partially insulated ring electrode in 0.1 M HCOONa / 0.033 M H_2SO_4 / 1×10^{-6} M Bi^{3+} with scan rate 1 mV/s. On the cathodic scan, we observed the interfacial potential along the ring electrode. Figure 6.3 displays the interfacial potential distribution of the ring electrode when the reference electrode was placed at the center and same plane of the ring electrode ($\beta = 0$) in the active state (+0.280 V) of the bistable regime. With the non-insulated ring, the interfacial potential was practically homogeneous along the entire ring (Figure 6.3(a)). However, on the partially insulated ring electrode, the interfacial potential at the edges of the insulator was higher than at other parts of the ring, see Figure 6.3(b). Due to the low local effective resistance and high current density at the edges, the interfacial potential at edges of insulator was higher than around the edges. In the passive state the interfacial potential of the ring with insulator was almost homogeneous; edge effects of the insulator did not manifest itself because whole the electrode was passivated completely anyway.

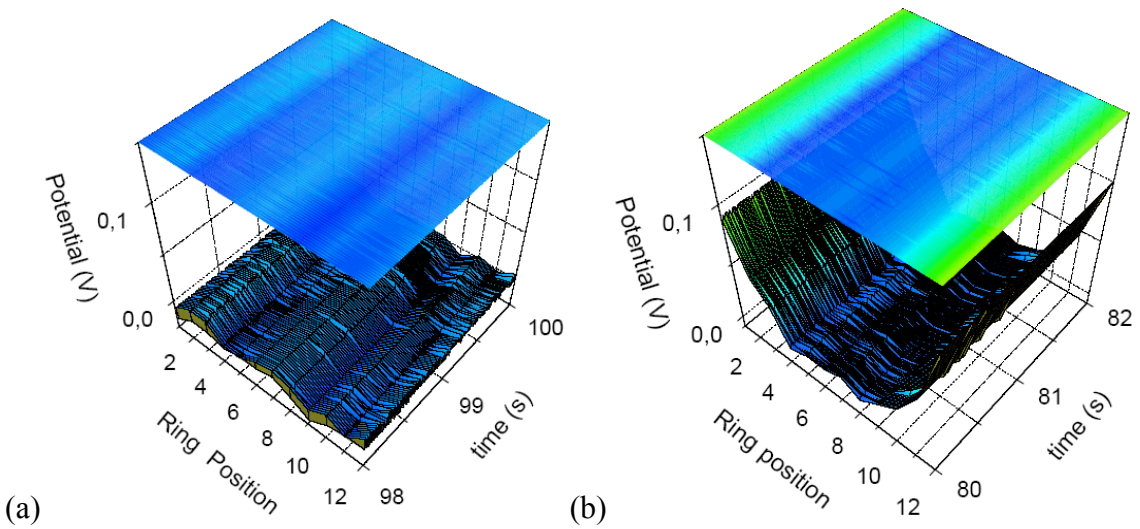

Figure 6.3. Stationary interfacial potential distribution on Pt ring electrode in the active state +0.280 V, the reference electrode placed at the same plane of the working electrode (β = 0). (a) non-insulated Pt ring electrode (b) insulated Pt ring electrode.

(B) Spatiotemporal pattern sequences in cyclic voltammetry

During cyclic voltammetry in 0.1 M HCOONa / 0.033 M H_2SO_4 / 1×10^{-6} M Bi^{3+} with scan rate 1 mV/s, a broader oscillatory region (as compared to the uninsulated ring) was observed on the cathodic scan (Figure 6.4), and also the current oscillations and pattern formation changed significantly depending on potential. At the onset of current oscillations, they were of period-1 and the pattern represented standing waves (in-phase at the edges of the insulator) shown in Figure 6.5(a). As the potential became higher, the current oscillations were period-1 like the beginning but pattern was changed from standing wave to travelling pulse waves reproduced in Figure 6.5(b). At higher potential aperiodic oscillations appeared. These were associated with anti-phase oscillations at the edges, with pulses propagating back and forth along the rest of the electrode. The irregularity of the overall oscillations were stemming from aperiodic creation and annihilation of these pulses (Figure 6.5(c)). Towards the end of the oscillatory region, the current oscillations had lower frequency and higher amplitude, associated with strong anti-phase oscillations at the edges see Figure 6.5(d)

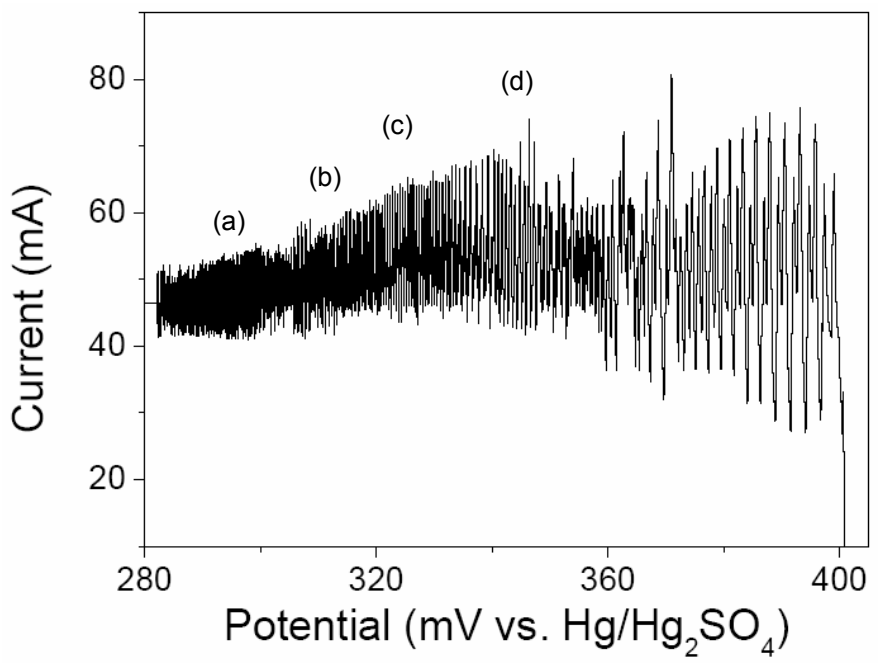

Figure 6.4. Current oscillations on partially insulated ring during cyclic voltammetry for the electro-oxidation of formic acid in presence of Bi^{3+} ions. Electrolyte is 0.1 M HCOONa / 0.033 M H_2SO_4, scan rate 1 mV/s (β = 0). (a) standing waves in-phase at edges, (b) pulses, (c) pulse propagation failure at insulator, oscillations out of phase at edges, and (d) anti-phase oscillations at edges.

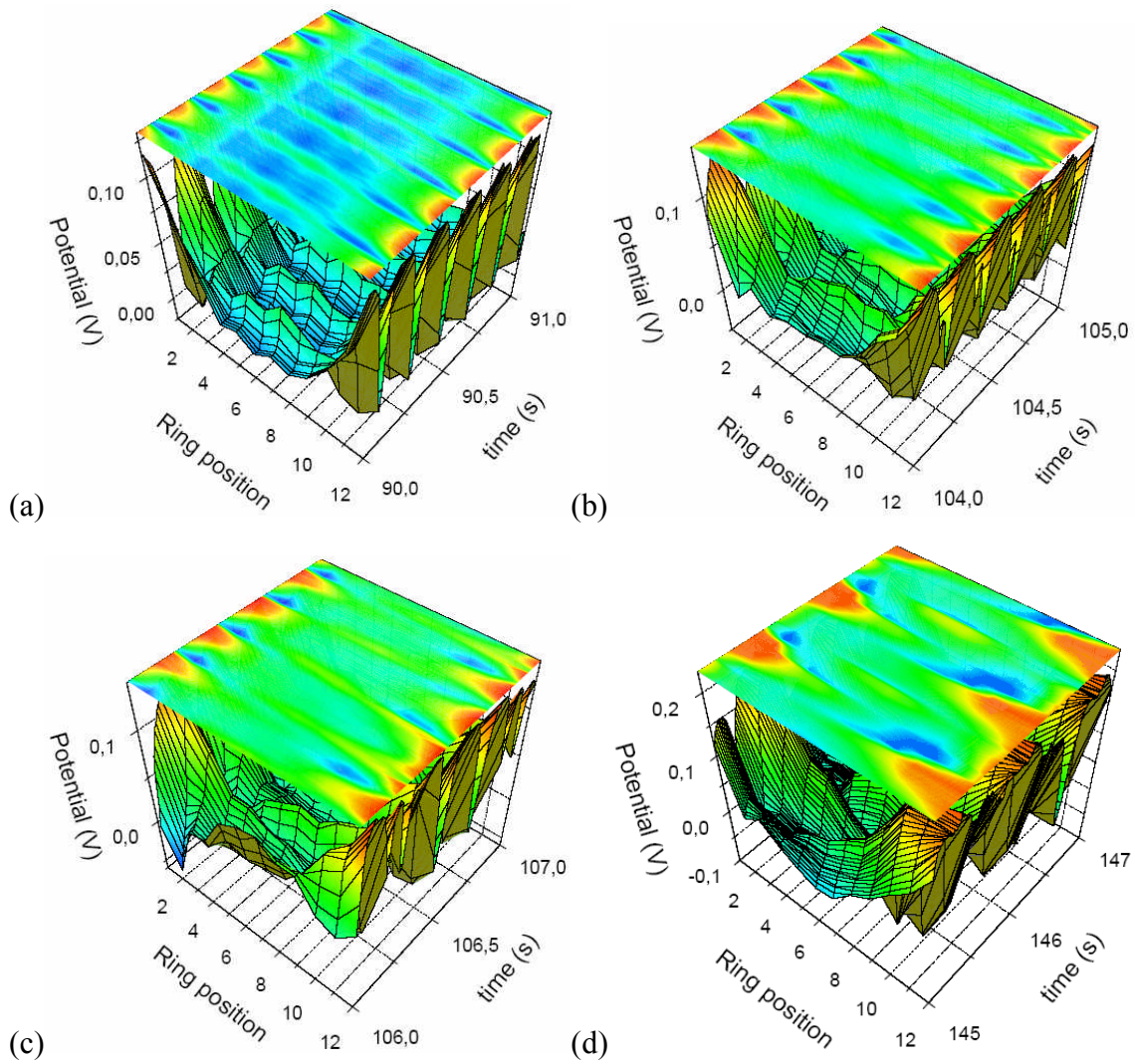

Figure 6.5. Spatiotemporal pattern formation for different potential during cyclic voltammetry (in Figure 6.4) with the reference electrode placed at the same plane of the partially insulated ring working electrode (β = 0, insulator at positions between 1 and 12). (a) +0.284 V, (b) +0.304 V, (c) +0.320 V, and (d) +0.343 V.

(C) Pattern formation at constant applied potential

Anti-phase oscillations of the interfacial potential at the edges of the insulator were strongly affected by the potential, as displayed in Figure 6.6. The measurements were obtained for decreasing the applied potential in the condition of the close reference electrode (β = 0). At the high value of applied potential (+0.404 V) in Figure 6.6(a), the

pattern was of large amplitude and low frequency anti-phase wave. At the lower applied potential (+0.350 V), anti-phase pattern was small and weak, and the frequency was very fast, Figure 6.6(b). Travelling pulses at constant potential will be discussed in sections 6.3.2 and 6.3.3.

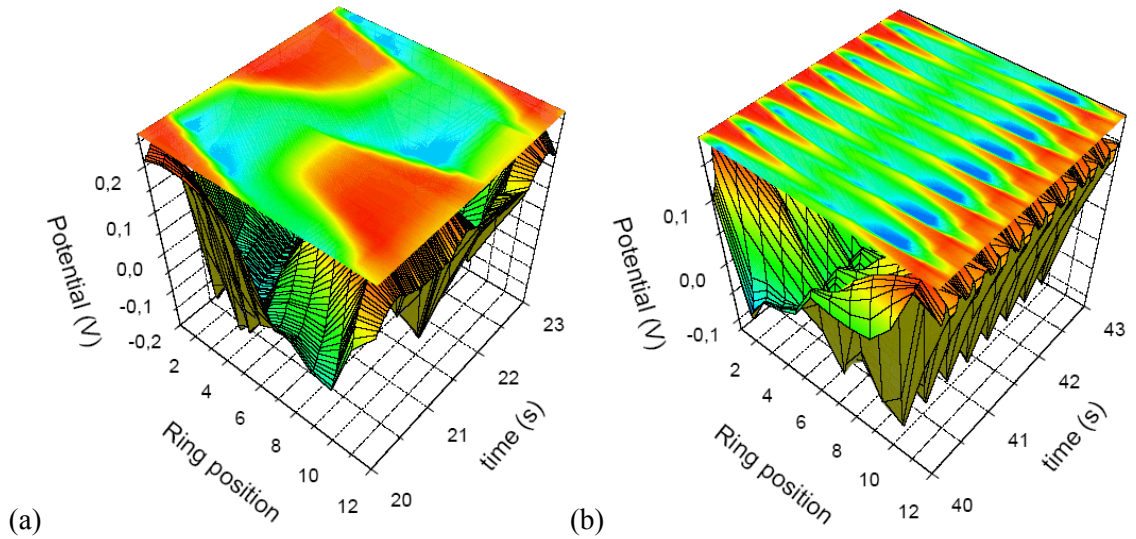

Figure 6.6. Spatiotemporal pattern formation for different potentials. (a) at +0.404 V and (b) at +0.350 V. Insulator at positions between 1 and 12.

(D) Pattern formation with increasing reaction time

Figure 6.7 shows the change of the pattern formation with increasing reaction time (*i.e.*, slowly decreasing formic acid concentration). The surface of the ring electrode became more passive state as the reaction continued. At the onset of current oscillations, they had small amplitude and high frequency and pattern consisted of small anti-phase waves. As the time passed, these anti-phase waves became more pronounced (like Figure 6.6(b)). After about 20 min, current oscillations had larger amplitude (Figure 6.7(a)), and the anti-phase oscillations from the both edges of the insulator were connected slightly along the ring (Figure 6.7(b)). The oscillations then became more synchronized (in-phase pattern formation). In the end, the current oscillation had large amplitude, and low frequency (Figure 6.7(c)). As can be seen from Figure 6.7(d), the whole ring was passive simultaneously, though the activation was not completely synchronized.

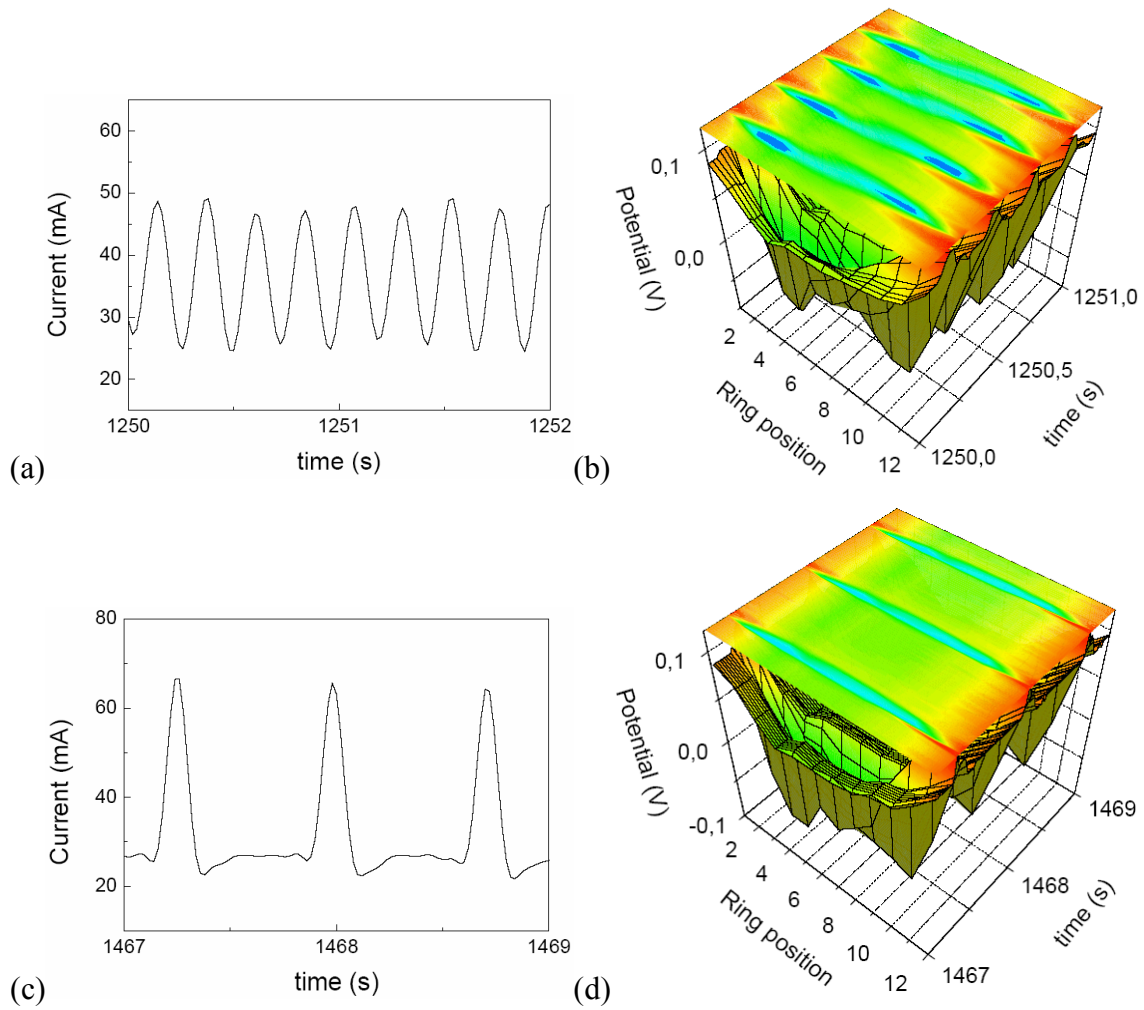

Figure 6.7. Current oscillations (a) and (c), spatiotemporal pattern formations (b) and (d) for each reaction time at the constant potential at +0.315 V. (a) and (b) at 1251 s, (c) and (d) at 1468 s. Insulator at positions between 1 and 12.

6.3.2 Travelling pulse waves and pulse reversal

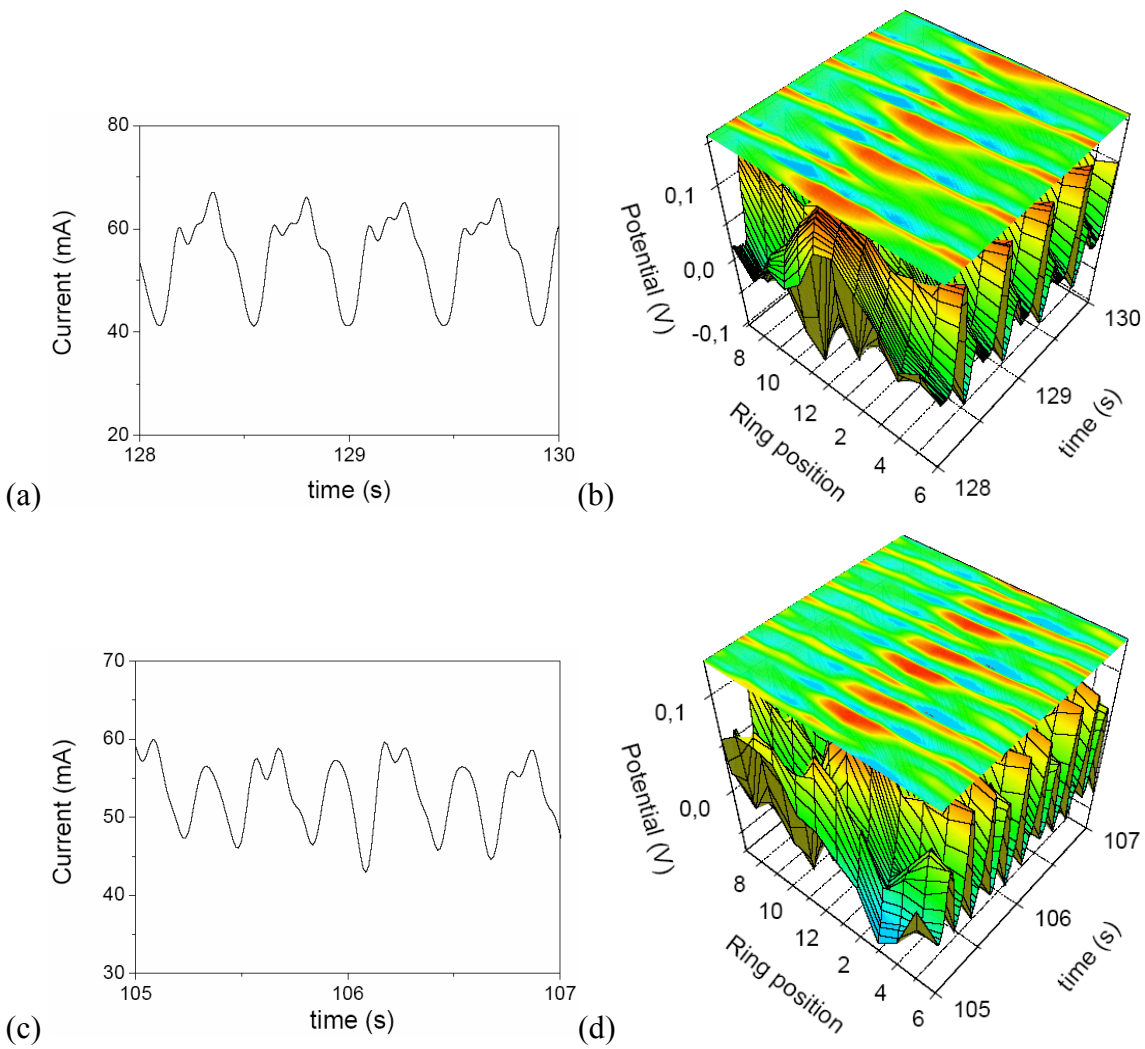

Figure 6.8. Current oscillations and travelling pulse waves at constant potential. Insulator at positions between 1 and 12. (a) and (b) are one-cycle travelling pulse waves at +0.320 V, (c) and (d) are two-cycle travelling pulse waves at +0.314 V.

With close reference electrode (β=0) and constant applied potential, various travelling pulse waves were observed. Besides simple travelling pulses, which locked the same at every rotation, (period-1 pulse *cf*. Figure 6.5(b) and Figure 6.9), these were also pulses which faded during one rotation and reappeared in full strength on the next rotation (most clearly discernible near the insulator). Thus Figure 6.8(a) and (b) show a pulse which vanishes practically completely when reaching the insulator at times

(128.25 + n 0.5)s to reappear at its next contact with the insulator (about 0.25s later) and remain discernible for the next full rotation (period-2 pulse). At slightly lower potential a period-3 pulse was obtained, which consisted of two strong and one weak pulse (Figure 6.8(c) and (d)).

Figure 6.9(a) and (b) show the current oscillation and the respective continuous (period-1) travelling pulse waves. During the pulse travelling, insulator had a more passive state than the other position in the passive domain. Clearly, the passive pulse jumped over the insulation part. This effect is described in more detail in the next section.

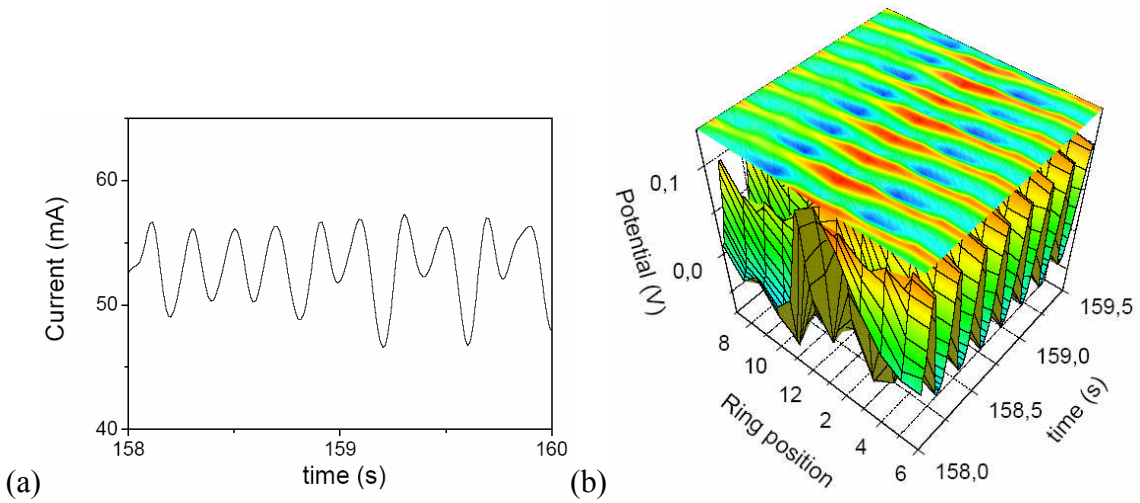

Figure 6.9. (a) current oscillations and (b) continuous travelling pulse waves at constant potential +0.314 V, the reference electrode placed in the same plane as the working electrode (β = 0).

Not surprisingly, the strong inhomogeneity induced by the insulated area could also lead to propagation failure and pulse reversal. These effects could be most readily studied by application of a constant potential and use of the depletion of formic acid as a very slow parameter drift. At first the pulses always jumped over the insulator, then occasional pulse reversals occurred, as shown in Figure 6.10(a) and (b), but also double reversals (Figure 6.10(c) and (d)) were observed, *i.e.*, the pulse changed direction at the insulator twice in a row restoring its original orientation. As time progressed these

events became more frequent. The resulting oscillations were predominantly not periodic, but could also settle into stable patterns, such as the one in Figure 6.10(e) and (f), where a double pulse reversal and a penetrating pulse alternate.

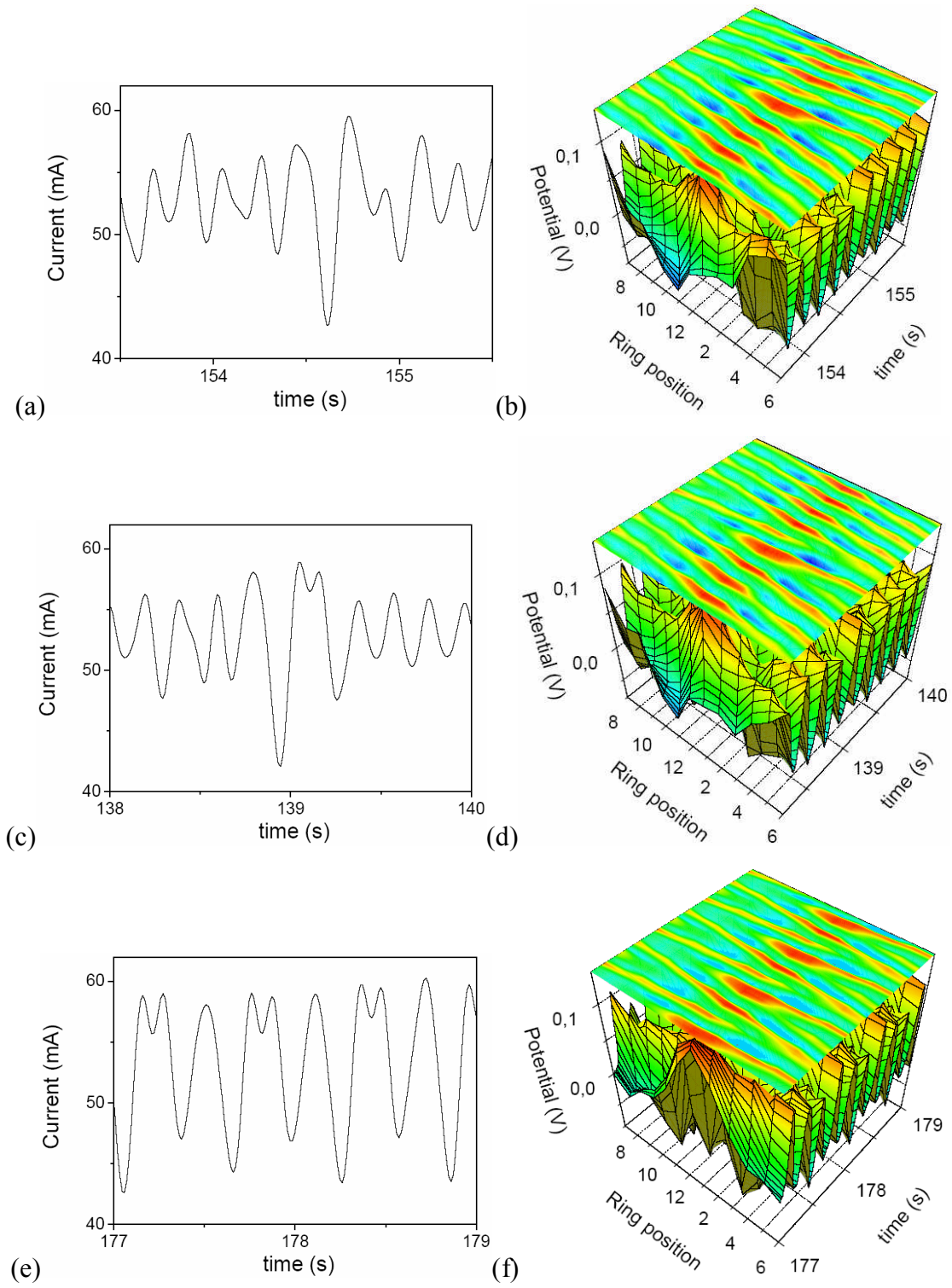

Figure 6.10. (a) and (b) are current oscillations and pattern formation of a single spontaneous pulse reversal. (c) and (d) are current oscillations and pattern formation of double spontaneous pulse reversal. (e) and (f) are current oscillations and pattern formation of a periodic pattern of one propagating pulse followed by a double pulse reversal.

6.3.3 Saltatory conduction of travelling pulse wave

A travelling pulse on a pure ring electrode had constant velocity (Figure 6.11(a)). Having an insulator on a ring electrode, the interfacial potential was temporally higher near the insulator than around that for the passive travelling pulse waves (in case of active travelling pulse waves, the interfacial potential was lower at the edge of the insulator). Travelling pulse could jump over the insulator, and continuously moved along the ring in Figure 6.11(b)-(e). Placing a very small (less than 3°) insulator had little effect, Figure 6.11(b). For larger insulator (5°-25°), the travelling pulse jumped over insulator with enhanced velocity. In contrast, a much larger insulator (above 30°) resulted in propagation failure of the pulse giving rise to standing-wave oscillations in Figure 6.11(f).

Space-time plots of the pulse position, in Figure 6.12, show the propagation behavior of the travelling pulse over the insulator in detail. These points are each position of the minimum interfacial potential (active pulse) above a ring. On pure and small insulator (3°) ring electrode in Figure 6.12(a) and (b), the velocity of the pulse was almost constant as discussed above. On an insulator of 5°, the velocity of the travelling pulse was strongly enhanced by the insulator when it approached from position 9 to one edge of the insulator (position 12) in Figure 6.12(c). With 10° of insulator, in Figure 6.12(d), the velocity of the pulse increased over about 4 positions before it arrived at one edge of the insulator, but this effect was discernible for only 1 position after the pulse jumped over the insulator. When the travelling pulse travelled over the 25° insulator in Figure 6.12(e), it got a strong effect for 4 positions before and after the insulator. Here, we could see a delay in the jump over the insulator. With a too large insulator (30°), no travelling waves could be observed any more, rather standing waves occurred with one node at the insulator (Figure 6.12(f)).

When we compared the ratio of velocity between the region in which the velocity was increased with insulator effect and the region without this effect (v_{α° = $v_{region\ with\ effect}$ / $v_{region\ without\ effect}$), the ratio of velocity increased as the angle of width of insulator became larger (v_{5° = 1.4, v_{10° = 1.5, v_{20° = 1.83 and v_{25° = 2.67). As the width of

the insulator increased, we could see clearly that the active travelling pulse got influence of the insulator over a wider region around it.

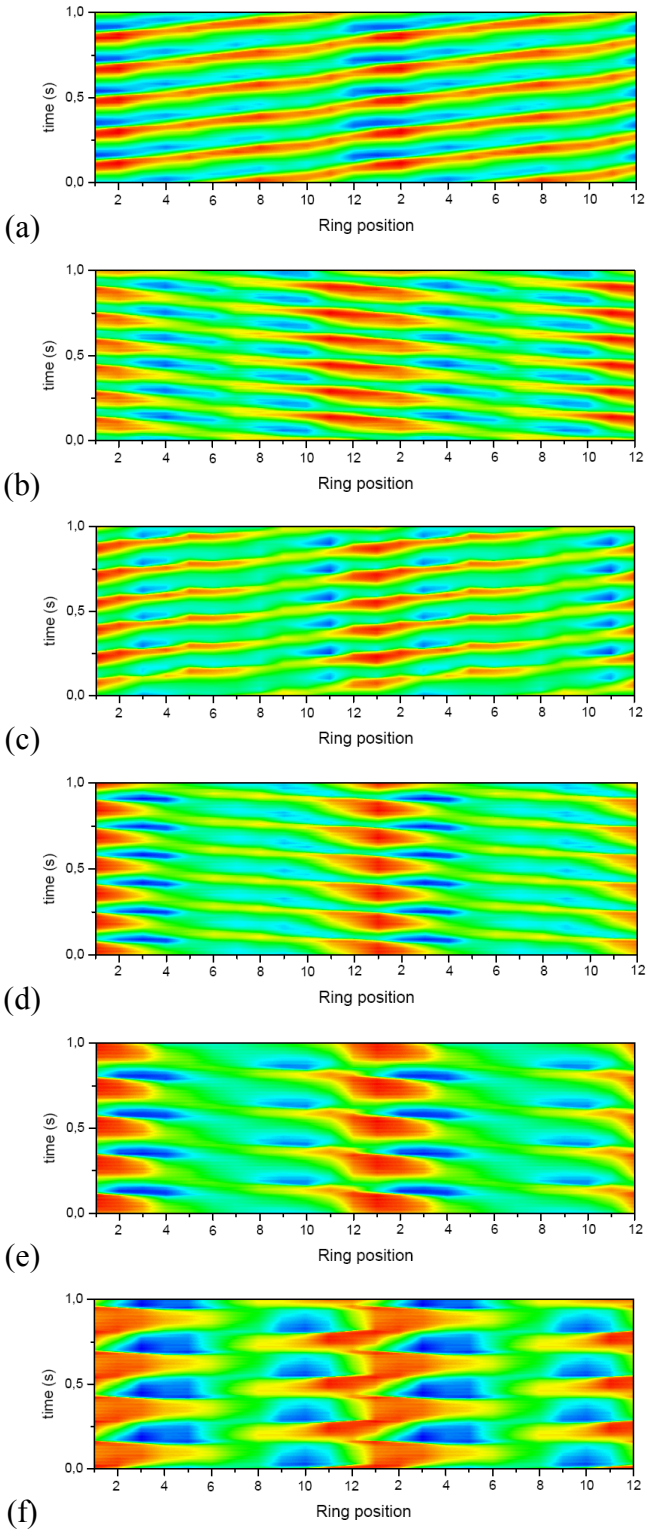

Figure 6.11. Travelling pulses on a ring electrode (blue-active, red-passive travelling pulse). The electrolye was 0.1 M HCOONa / 0.033 M H_2SO_4 / 1×10^{-6} M Bi^{3+} (β = 0). (a) Pure ring electrode at +0.207 V, (b) 3° insulator at +0.212 V, (c) 5° insulator at +0.314 V, (d) 10° insulator at +0,183 V, (e) 25° insulator at +0.203 V. (f) 30° insulator at +0.222 V.

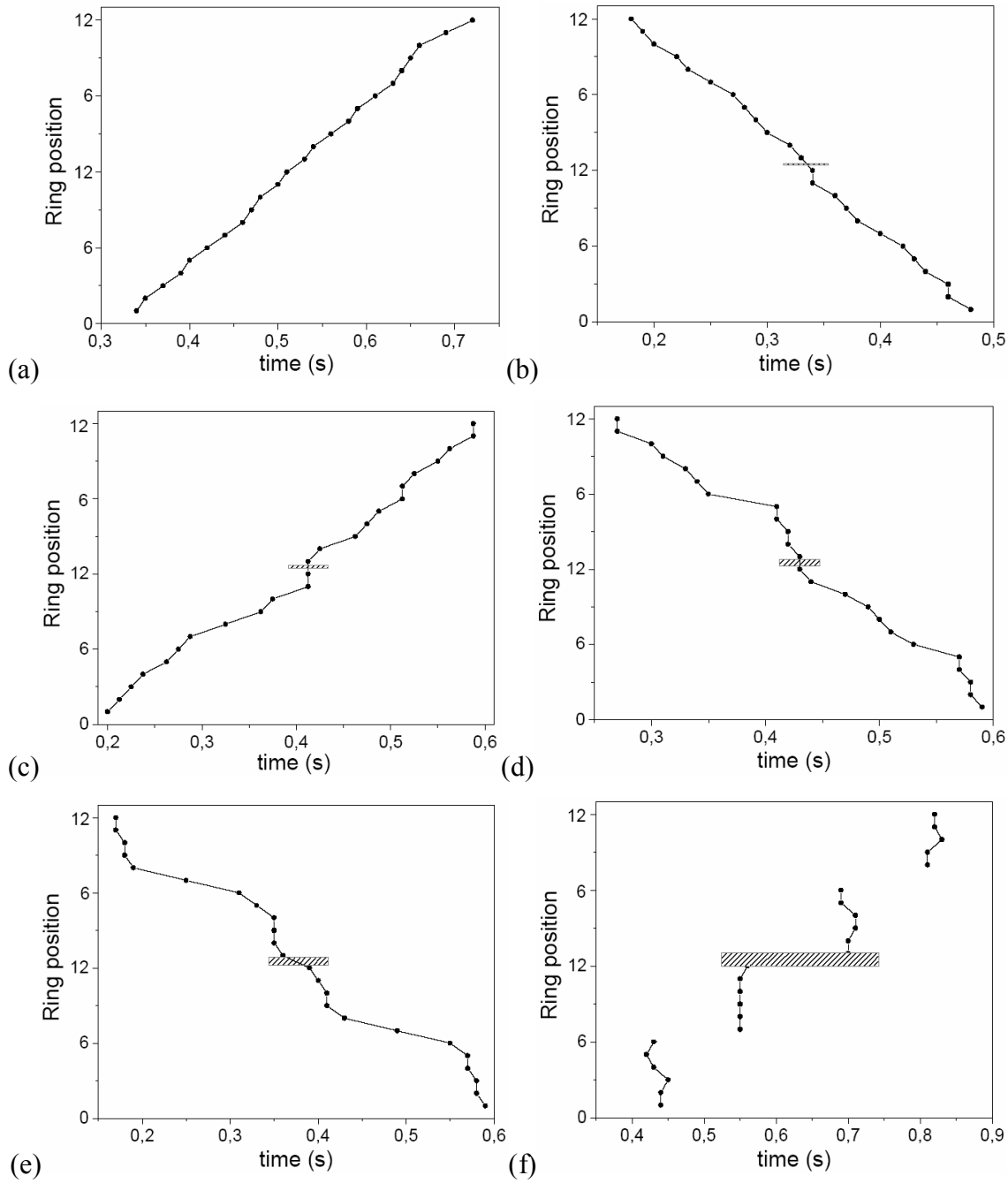

Figure 6.12. Space-time plot of active travelling pulse from Figure 6.11. Each point means the movement of the active travelling pulse along the ring electrode. The position and width of the insulator are marked as shaded areas.

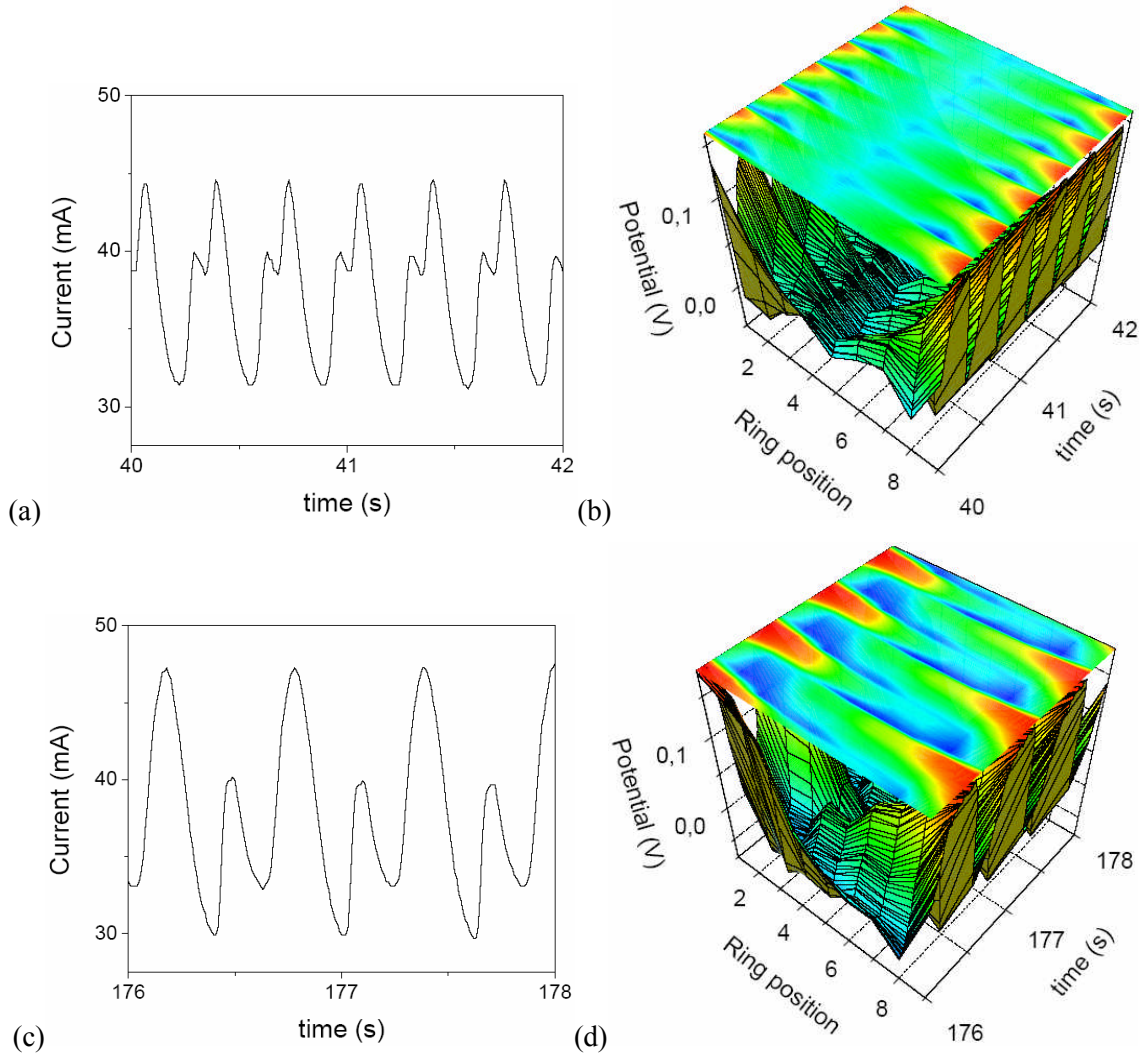

Figure 6.13. Spatiotemporal pattern formation with 90° width of insulator (β = 0) at +0.219 V. After reaction time of (a) 40 s, (b) 170 s.

When the width of insulator was 90° (between positions 9 and 1), anti-phase standing wave pattern formations were observed as shown in Figure 6.13. At the beginning, small anti-phase edge oscillations were observed (Figure 6.13(a) and (b)). After 170 s the anti-phase edge oscillations became stronger, *i.e.*, penetrated more of the ring (Figure 6.13(c) and (d). In this system, we could not observe any travelling pulse waves.

When the width of insulator was much larger (180° between positions 6 and 1), again anti-phase oscillations were observed at the edges (Figure 6.14(a) and (b)). With time the associated pattern looked rather like a back-and-forth movement along the uncovered ring (Figure 6.14(c) and (d)); finally the oscillations became almost synchronized (Figure 6.14(e) and (f)). Overall, the behavior with 90° and 180° of insulated area were very similar to a ribbon electrode with not too large β [21].

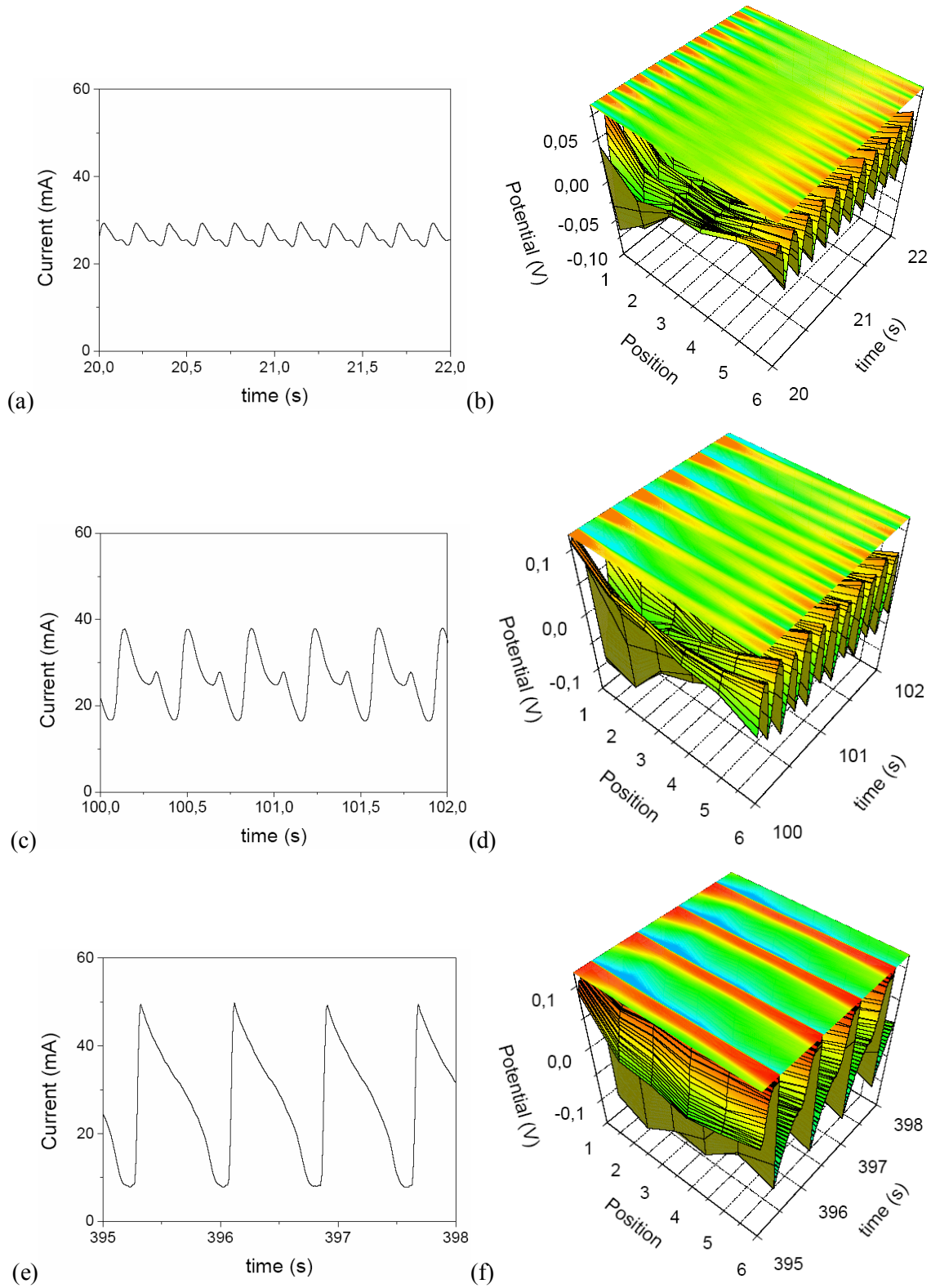

Figure 6.14. Spatiotemporal pattern formation with 180° width of insulator (β = 0) +0.261 V. Variation with reaction time (a) 20 s, (b) 100 s, (c) 390 s.

6.3.4 Pattern formation with large distance of reference electrode (β = 0.5)

When the distance between the working electrode and the reference electrode is increased (large β), the pattern formation became qualitatively different from the condition of the close reference electrode (small β). At constant applied potential (+0.429 V) and with a large distance between the working electrode and the reference electrode (β = 0.5), current oscillations and pattern formation were observed as shown in Figure 6.15. Firstly, period-1 oscillations occurred and the interfacial potential became immediately synchronized in space in Figure 6.15(a) and (a'). As time passed, the oscillations changed to the period-2. The corresponding pattern consisted of a large oscillation stretching to a considerable distance away from the insulator, followed by a smaller one occurring just near the edges (1^1 pattern). Over time, the large oscillation penetrated further and further along the ring, while at the same time more and more smaller edge oscillations appeared (patterns 1^2, 1^4 and 1^5 in Figure 6.15(c), (d) and (e), respectively). Finally, at least the large oscillations covered the whole ring, interspersed by a varying number of smaller oscillations. The resulting complex aperiodic pattern is reproduced in Figure 6.15(f).

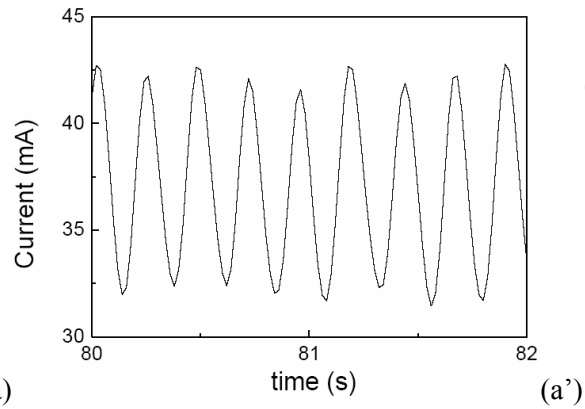
Current (mA)
time (s)
45
40
35
30
80
81
82

(a)

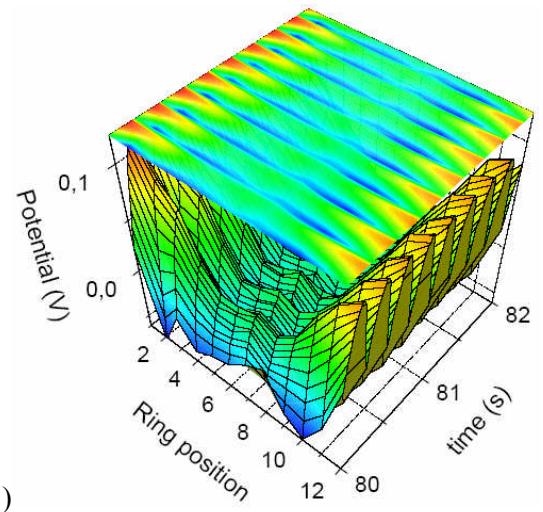
Potential (V)
0,1
0,0
Ring position
2
4
6
8
10
12
time (s)
80
81
82

(a')

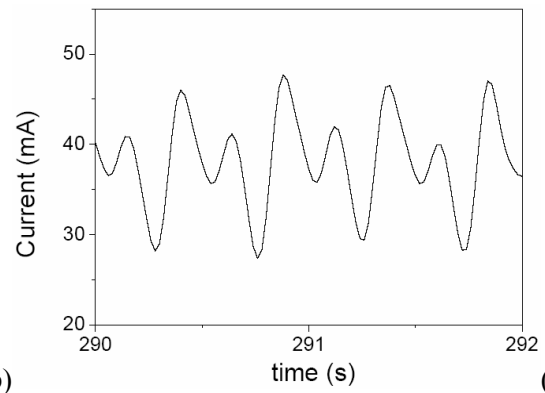
Current (mA)
time (s)
50
40
30
20
290
291
292

(b)

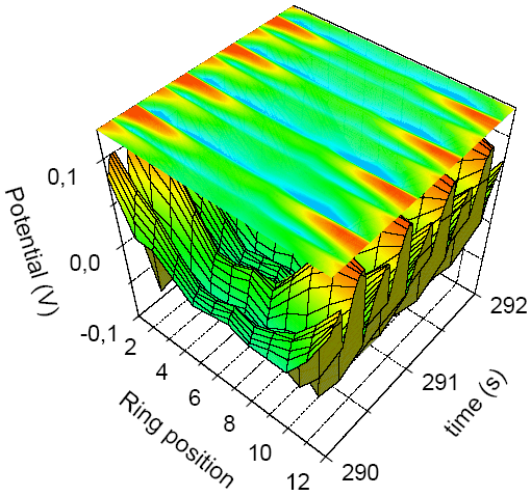
Potential (V)
0,1
0,0
-0,1
Ring position
2
4
6
8
10
12
time (s)
290
291
292

(b')

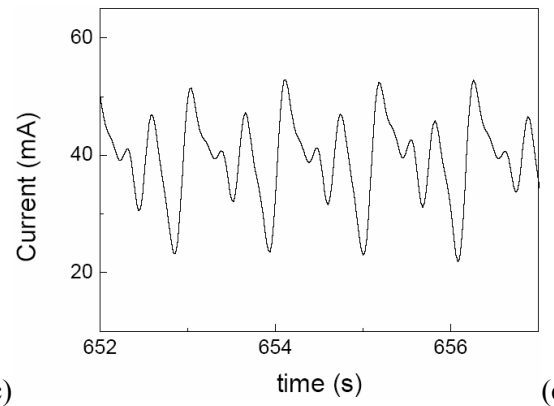
Current (mA)
time (s)
60
40
20
652
654
656

(c)

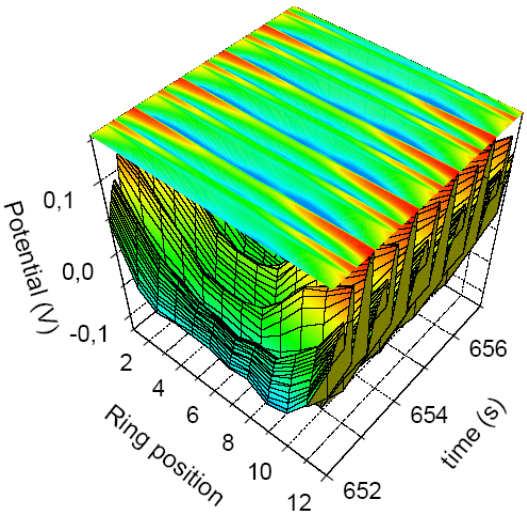
Potential (V)
0,1
0,0
-0,1
Ring position
2
4
6
8
10
12
time (s)
652
654
656

(c')

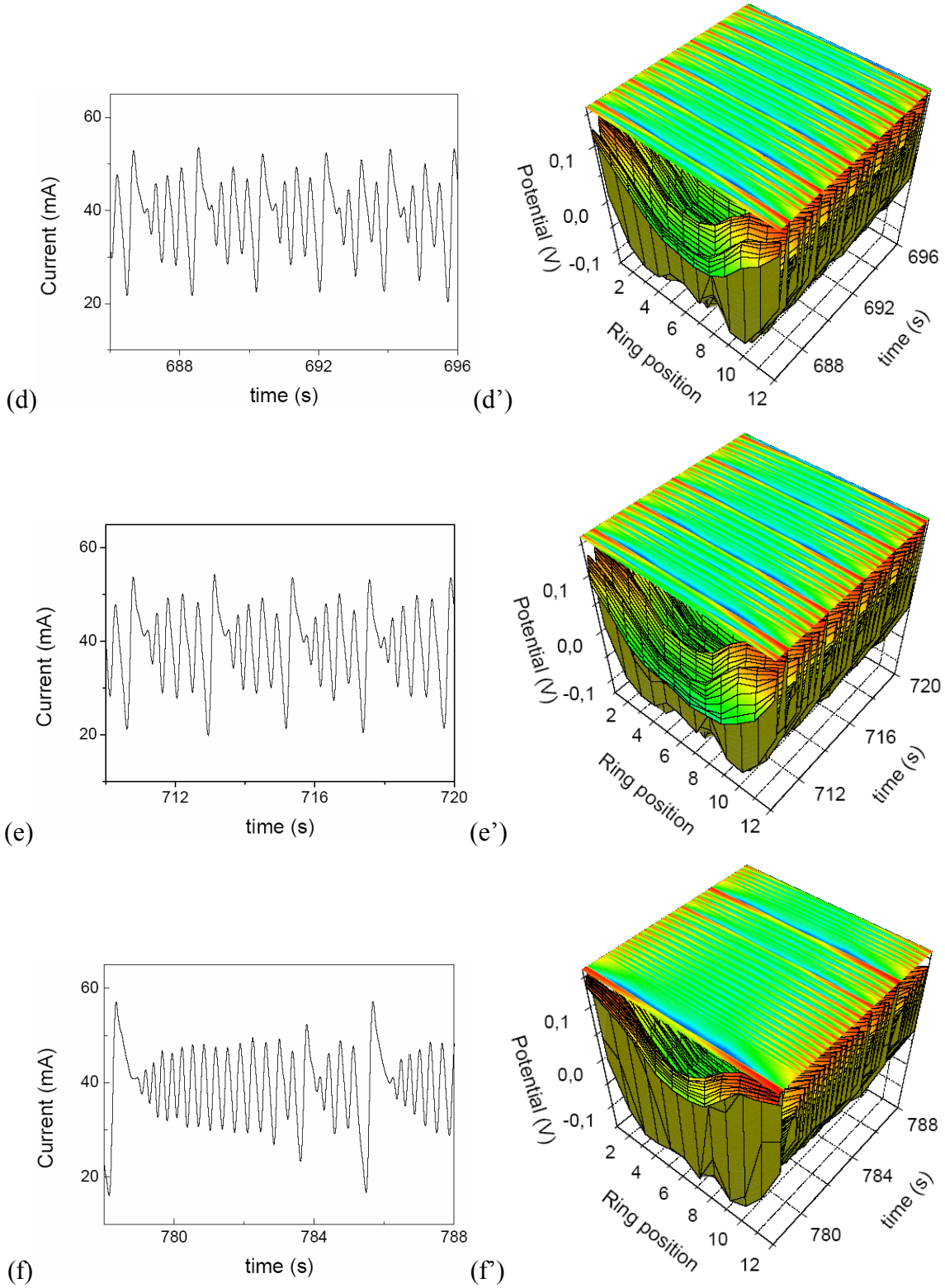

Figure 6.15. Time series of current oscillations and spatiotemporal pattern formation corresponding the current profile at constant potential (+0.429 V), the reference electrode is far away from the working electrode (β = 0.5). Insulator area 5° between positions 12 and 1.

6.3.5 Pattern formation with two & three insulated areas ($\beta = 0$)

(a) Two-insulator system

The schematic view of the experimental set-up is shown in Figure 6.16. The WE was the polycrystalline platinum ring electrode with inner diameter of 34 mm and outer diameter of 40 mm. Parts of the electrode were insulated between positions 12 and 1, 6 and 7 (180° separated two insulated regions) by coating with Apiezon wax over an angle 5°. All the other conditions were the same as in the former experiments.

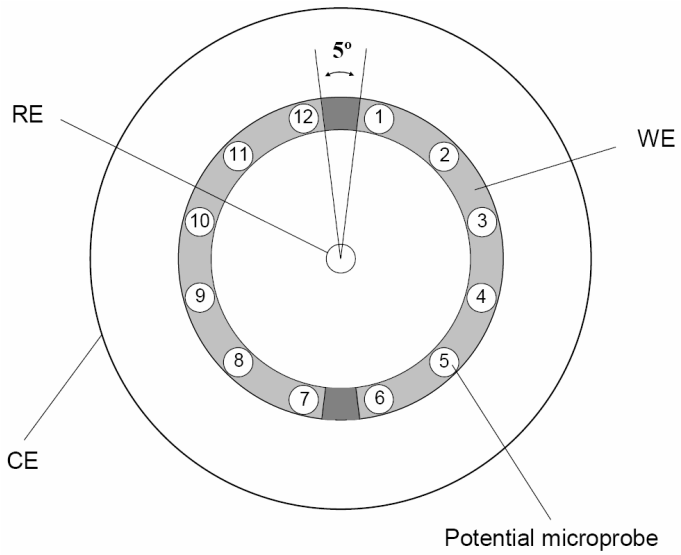

Figure 6.16. Schematic view of the experimental setup. Two-part insulator ring electrode. Insulators are Apiezon wax of 5° width.

For low potential (below +0.2 V) the essential sequence of patterns with the 2-insulator system was the same as on a ring without or with one insulator. This is shown in Figure 6.17, where the oscillations start as standing waves in-phase at edges belonging to the same insulated area, turn into travelling pulses, and then switch to anti-phase oscillations in which the insulators act as nodes (anti-phase edges).

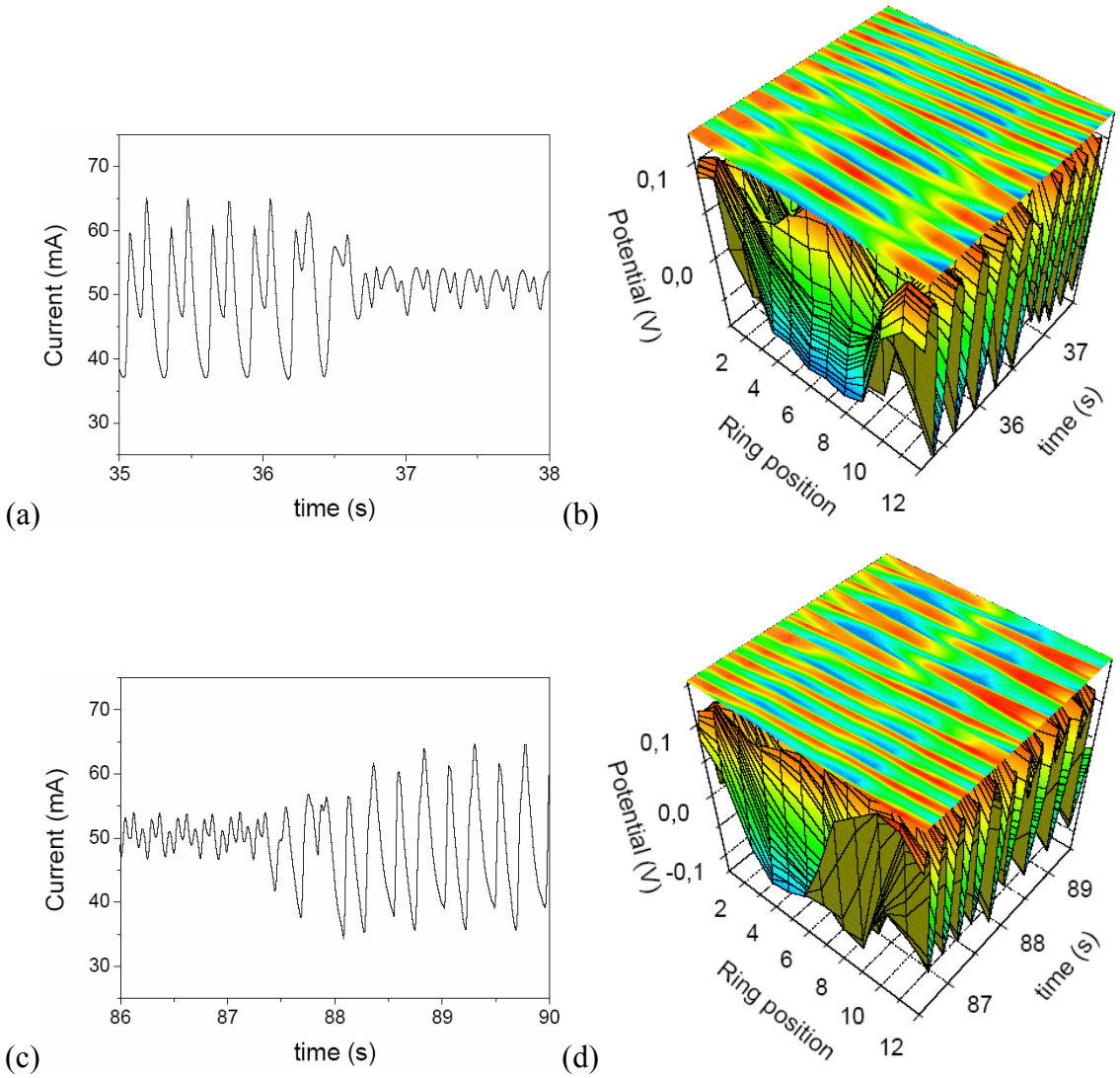

Figure 6.17. Time series of the current oscillations (a) and (c), and spatiotemporal pattern formation (b) and (d) at constant potential +0.173 V. Pattern formation changed from standing wave to travelling pulse and anti-phase wave (β = 0).

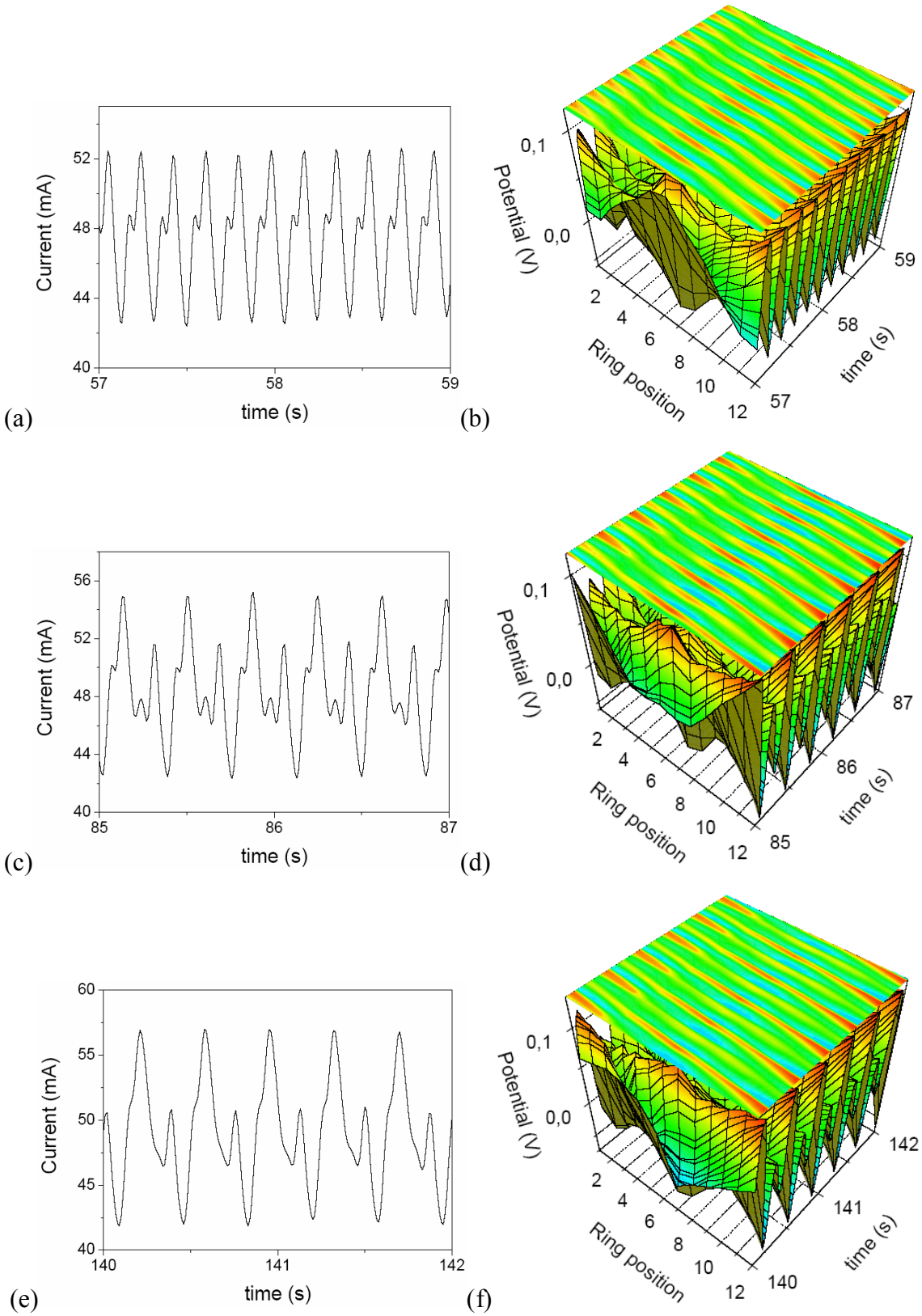

Figure 6.18. Change of the pattern formation of travelling pulse wave at constant potential +0.178 V as the reaction time passed (β = 0).

The travelling pulses were studied in some more detail at slightly higher potential (+0.178 V). As can be seen from Figure 6.18(a) and (b), a period-1 pulse was associated with a characteristic current oscillation (reflecting the insulators and any other inhomogeneities of the ring). Period-doubled pulses are reproduced in Figure 6.18(c) and (d), the less pronounced pulse is also clearly discernible in the lower amplitudes of the current oscillations. After yet longer reaction time the smaller current peaks had degenerated into shoulders (Figure 6.18(e)) but the pulse remained of period-2 (Figure 6.18(f)). Note that, unlike the case with only 1 insulator, the pulse never faded so as to become indiscernible, but always remained clearly visible.

In the 2-insulator system, saltatory conduction of a travelling pulse over the insulators was observed as in the system with 1 insulator (Figure 6.11(c)). In Figure 6.19(a), the effect of 2 insulators (between positions 6 and 7, as well as 12 and 1) is clearly visible in the shape and velocity of the pulse. The velocity changes become more apparent in the space-time plot of Figure 6.19(b).

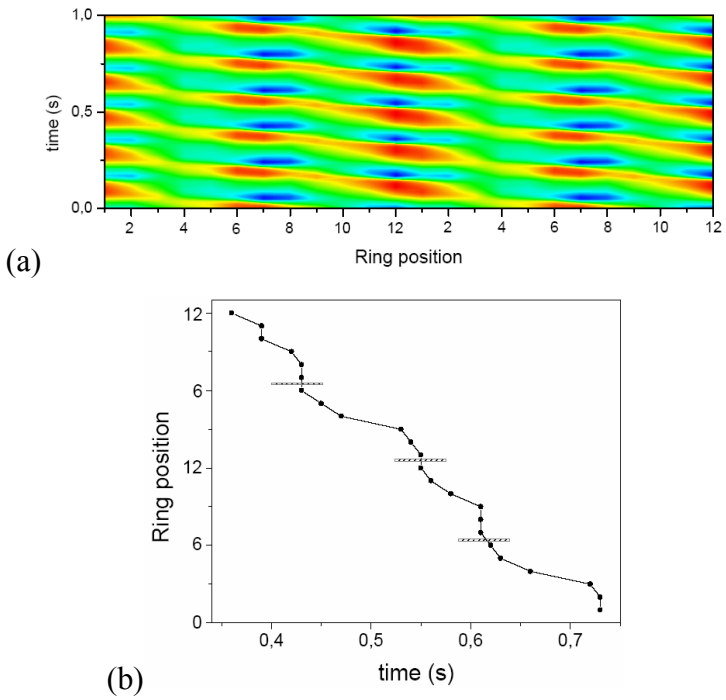

Figure 6.19. (a) Pattern formation of travelling pulse wave above the insulator and (b) space-time plot of passive (maximum interfacial potential) travelling pulse (β = 0). The conditions are same as in Figure 6.18. Insulated areas are marked by the shaded bars in (b)

At higher anodic potential (above about +0.22 V), the current oscillations were aperiodic and exhibited high amplitude. As the reaction time passed (6 s) this current oscillatory form changed to small amplitude oscillations in Figure 6.20(a) and (c); half of surface (between positions 7 and 12) was deactivated (Figure 6.20(b) and (d)) and exhibited only small oscillations and small spatial variations, while the other half (between positions 1 and 6) was in the active state with more pronounced temporal and spatial variations. This trapped pattern formation had not been observed with just one insulated area.

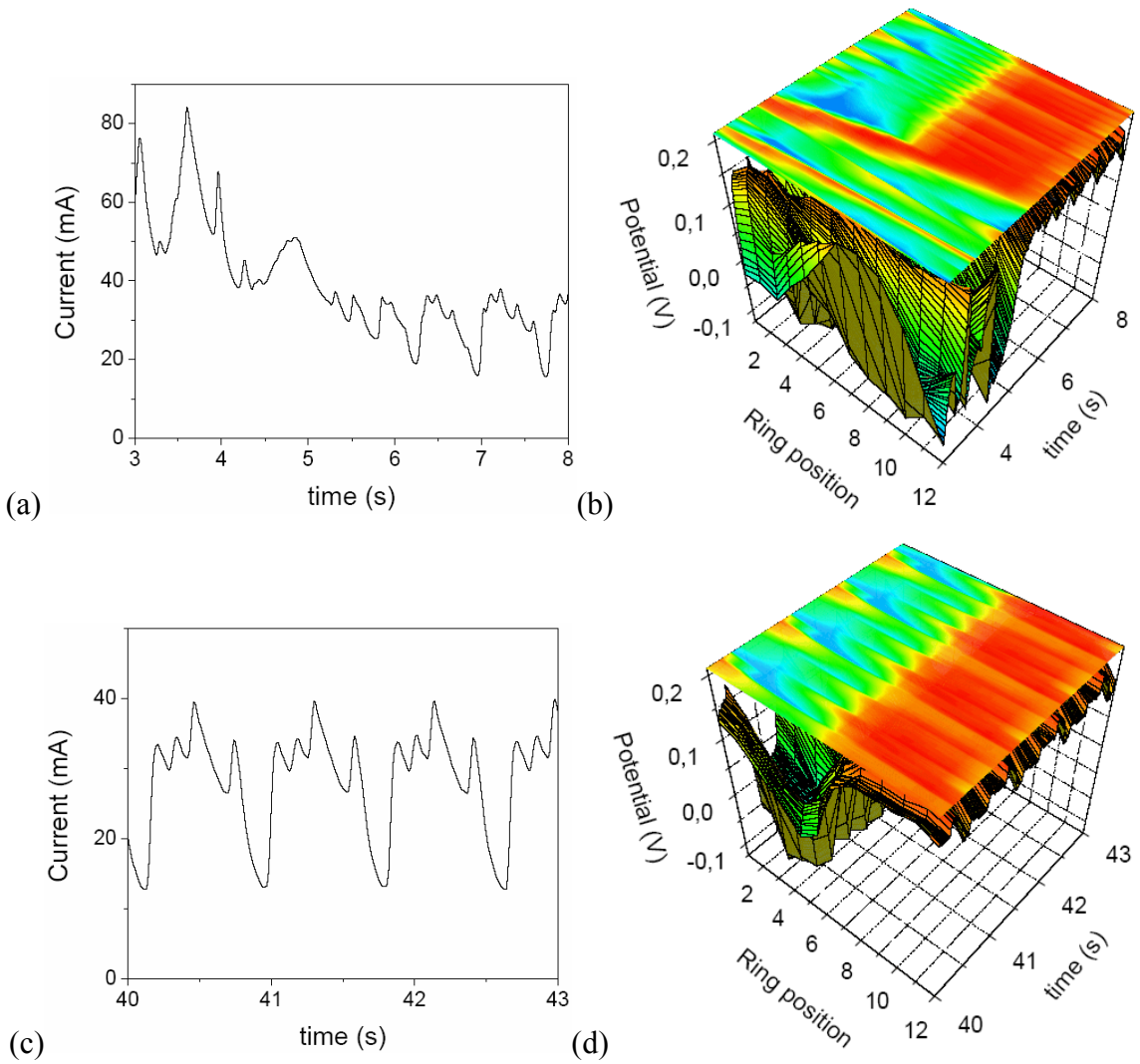

Figure 6.20. (a) and (c) Current oscillations, (b) and (d) Trapped pattern formation at constant potential +0.231 V (β = 0).

(B) Three-insulator system ($\beta = 0$)

The schematic view of the experimental setup is shown in Figure 6.21. Parts of the electrode were insulated between positions 12 and 1, 4 and 5, 8 and 9 (120° separated three insulated regions) by coating with Apiezon wax over an angle of 5°. All the other conditions were the same as in the former experiments.

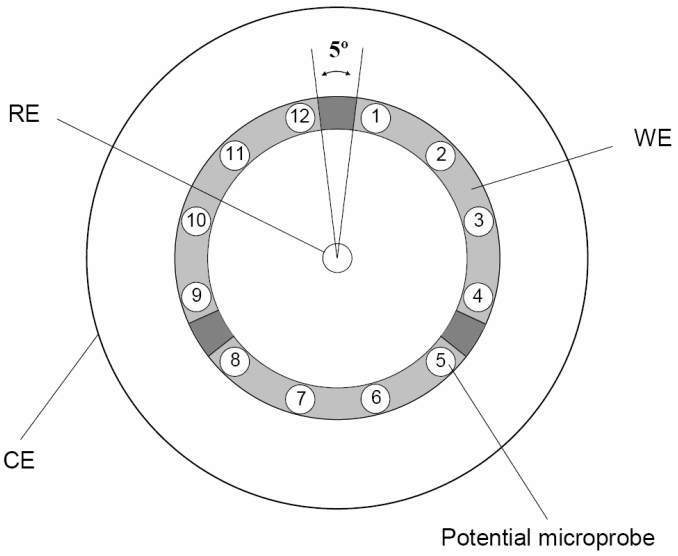

Figure 6.21. Schematic view of the experimental setup. Three-part insulator ring electrode. Insulators are Apiezon wax of 5°.

In addition to the introduction of edge effects, this arrangement of insulated areas with 3-fold rotational symmetry is not compatible with one of the basic patterns observed with 1 and 2 insulators at low potential, namely standing waves in-phase at the edges of a given insulator with nodes 180° apart.

There are two basic ways out of this predicament; either the system insists on adjacent edges being in-phase (dividing the ring into phase domains of ⅔ and ⅓ instead of ½ and ½), or it keeps the nodes 180° apart, in which case one node will be located at an insulator. Both possibilities were realized under very similar conditions as shown in Figure 6.22. In Figure 6.22(b) (+0.173 V) there are nodes between positions 2-3 and 10-11, all edges of a given insulator oscillate in-phase. The smaller phase domain (positions

11-2) exhibits higher amplitude, probably to compensate for its smaller size. In contrast, the standing waves in Figure 6.22(d) (+0.168 V) maintain an equal division of the ring into phase domains with nodes at positions 6-7 and 12-1, but here the edges of the insulator between 12 and 1 have to be out-of-phase (despite strong coupling).

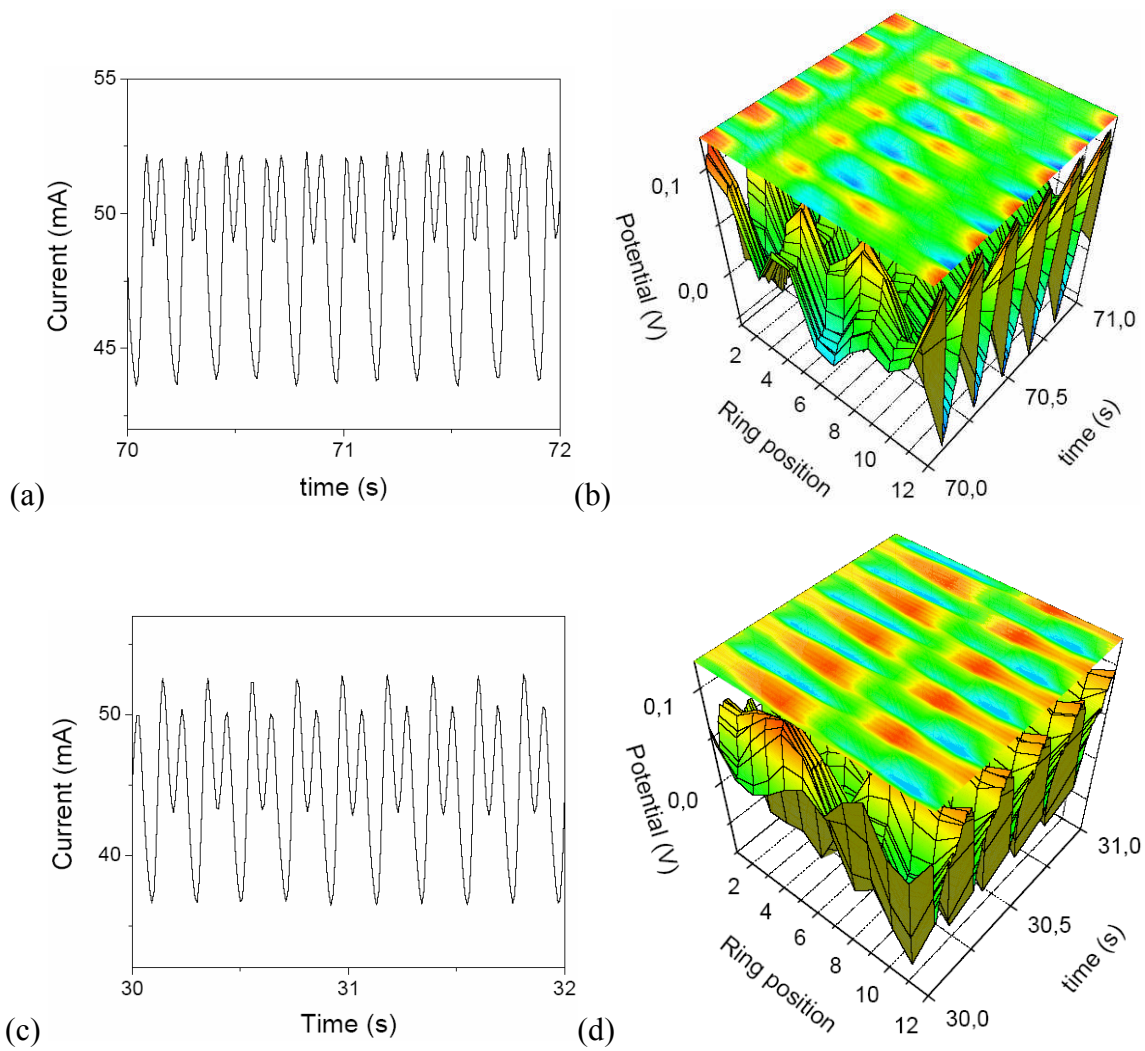

Figure 6.22. (a) Current oscillations and (b) spatiotemporal pattern formation of standing wave at constant potential +0.173V. (c) Current oscillations and (b) spatiotemporal pattern formations of standing wave at constant potential +0.168 V (β = 0). Insulator between positions 12 and 1, 4 and 5, as well as 8 and 9.

For slightly higher voltage (+0.183 V) a travelling pulse was obtained which again jumped over the insulated areas (Figure 6.23). In this case (3 insulators) the effect of the edges on the local voltage were very small, presumably because almost the entire electrode was affected by the edges, therefore the velocity of the pulse was almost constant as shown in Figure 6.23(c).

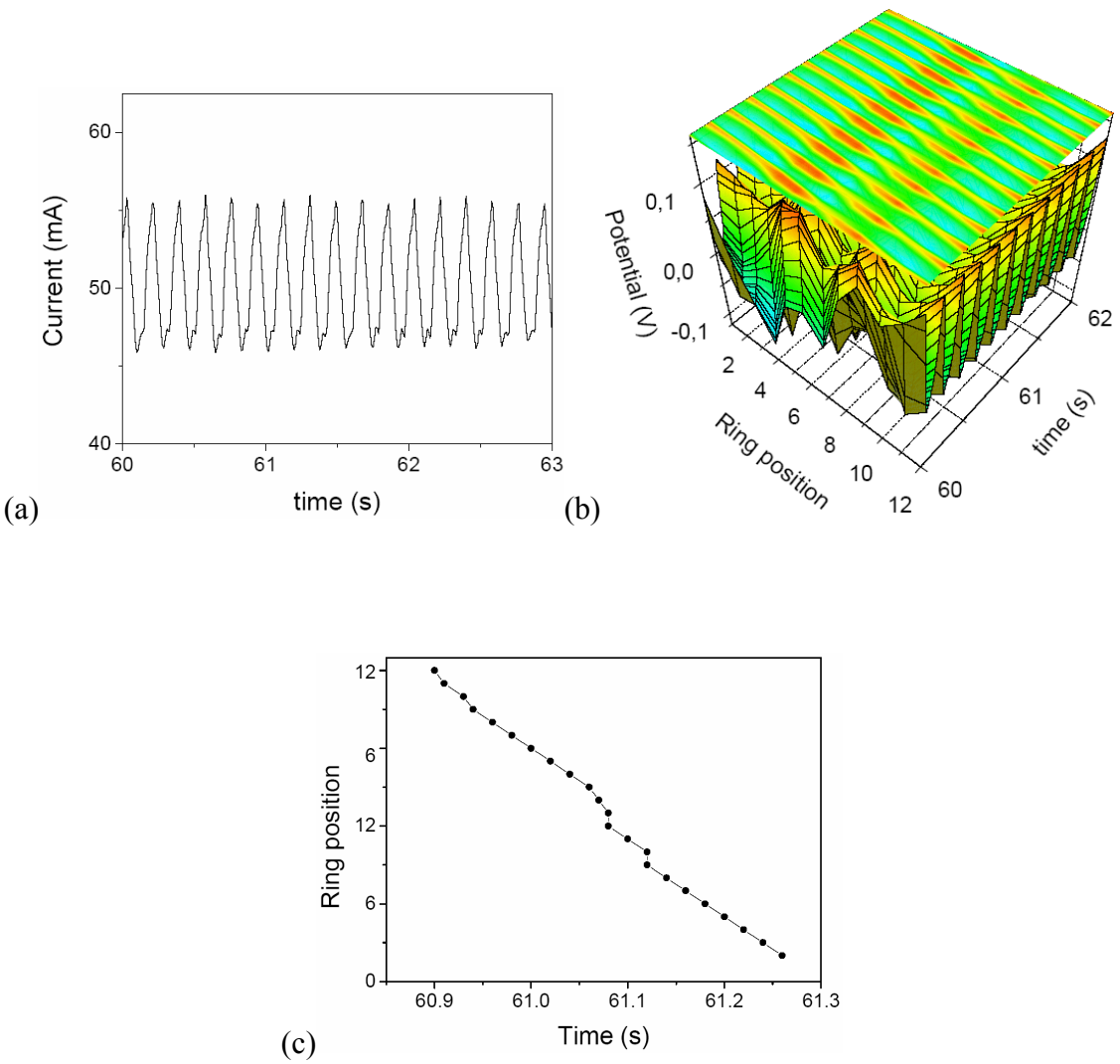

Figure 6.23. (a) Current oscillations and (b) spatiotemporal pattern formation of continuous passive (maximum interfacial potential) travelling pulse wave at constant potential +0.183 V. (c) space-time plot for the travelling pulse (β = 0).

At higher potential +0.188 V, the current showed period-3 oscillations (Figure 6.24(a)) and the passivation in one rotation strongly affected the positions 5-8, in the next rotation the other positions. The pattern is still moving, although it faded away almost completely in between (Figure 6.24(b)). Therefore it can be classified as a period-2 travelling pulse (*cf.* period-doubled pulses in the cases of 1 and 2 insulator above).

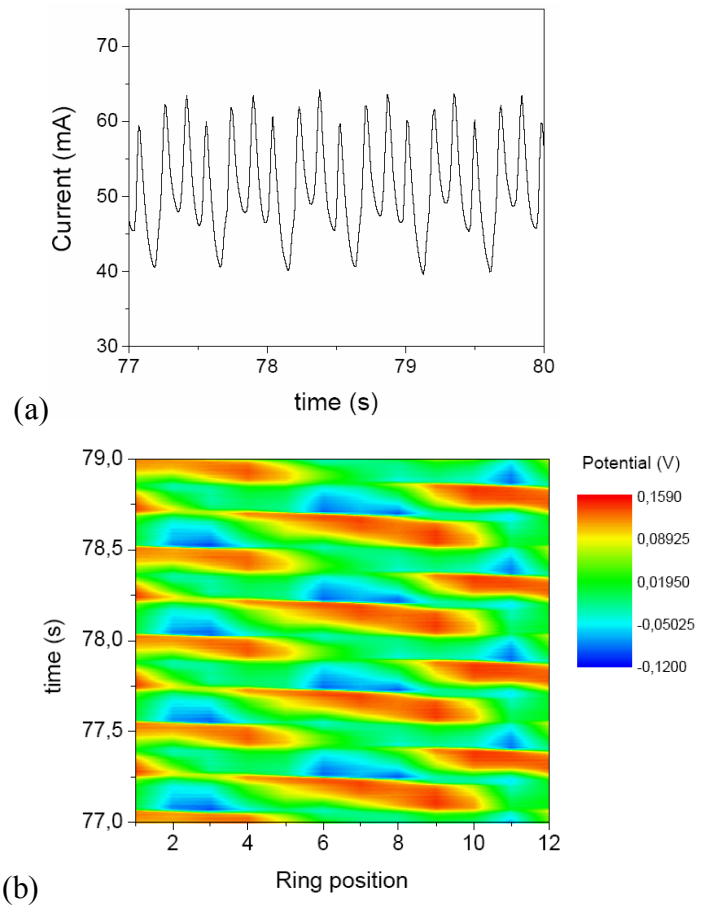

Figure 6.24. (a) Current oscillation and (b) spatiotemporal pattern formation of a period-2 travelling pulse wave at constant potential +0.188 V (β = 0).

At much higher anodic potential range at +0.212 V, trapped oscillations and pattern formations were observed, as shown in Figure 6.25. Of the three areas, just one area was in the passive state (deactivated) and other two areas were active state (activated). Mostly the area trapped in the passive state remained stationary, but

sometimes it moved periodically, mediated by a pulse travelling through the area in between (Figure 6.25(b)).

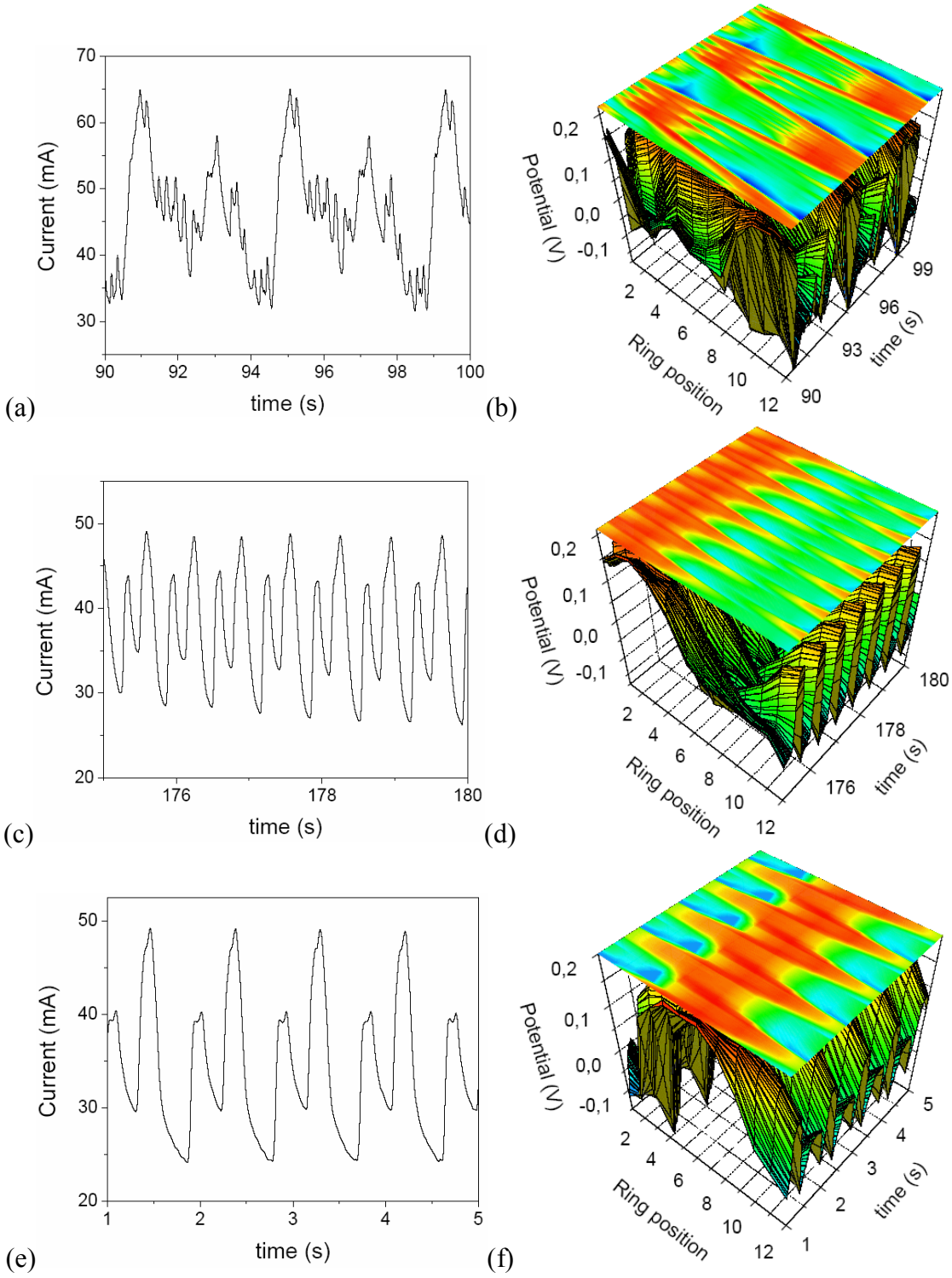

Figure 6.25. (a),(c) and (e) Current oscillations and (b), (d) and (f) Trapped pattern formation at constant potential +0.212 V (β = 0).

Yet another pattern was observed, which at first appeared to be travelling (Figure 6.26(c), to left side) and then settled into a stable oscillation consisting of 3 domains out of phase by ⅔π with each other. Note that these domains are not separated by the insulated areas but rather are asymmetrically centered around them. One could therefore also consider this pattern as a pulse jumping from around an insulated area to the next.

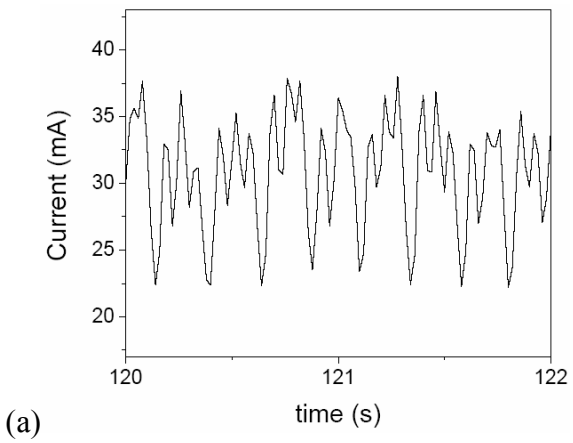

(a)

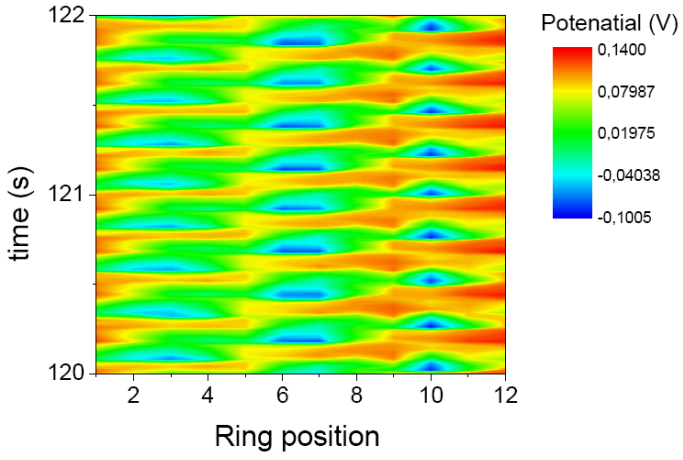

(b)

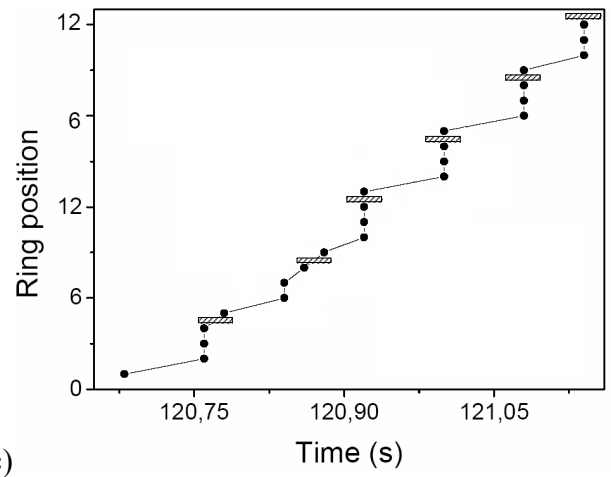

(c)

Figure 6.26. (a)Current oscillations, (b) travelling pulse wave with delay time in three insulators, and (c) space-time plot of passive (maximum interfacial potential) travelling pulse at constant potential (+0.241 V).

6.3.6 Autonomous transition from passive to active state on partially insulated ring electrodes ($\beta = 0$)

The bistability region is terminated by autonomous transition during the cyclic voltammetry. Here, we consider the transition from the passive to the active state in the bistable region. In our bistable system, firstly, the passive state was metastable and the active state was the globally stable state. During the cathodic scan with scan rate of 1mV/s, at one position a fluctuation drove the system locally to the active state, which expanded at the expense of the passive state. Figure 6.27(a) show the time trace of the total current and spatiotemporal pattern formation of interfacial potential during the transition on the one-insulator electrode. The activation fronts started from the middle at maximum distance from the insulator and then travelled to the edge of the insulator. On the two-part insulator electrode (insulators at position 12-1 and 6-7), in Figure 6.27(b), active fronts started at the position 9-10 and then, at the position 3-4 an active nucleus occurred. On three-part insulator electrode (insulators at position 12-1, 4-5 and 8-9), the 3 areas activated successively (Figure 6.27(c)). In Figure 6.28, more detailed active fronts are shown, they also started in the middle between 2 insulators (position 10-11, 2-3 and 6-7). Similar results were shown in the ribbon electrode system [21], in this system active fronts occurred at the center of the ribbon electrode (middle of both edges).

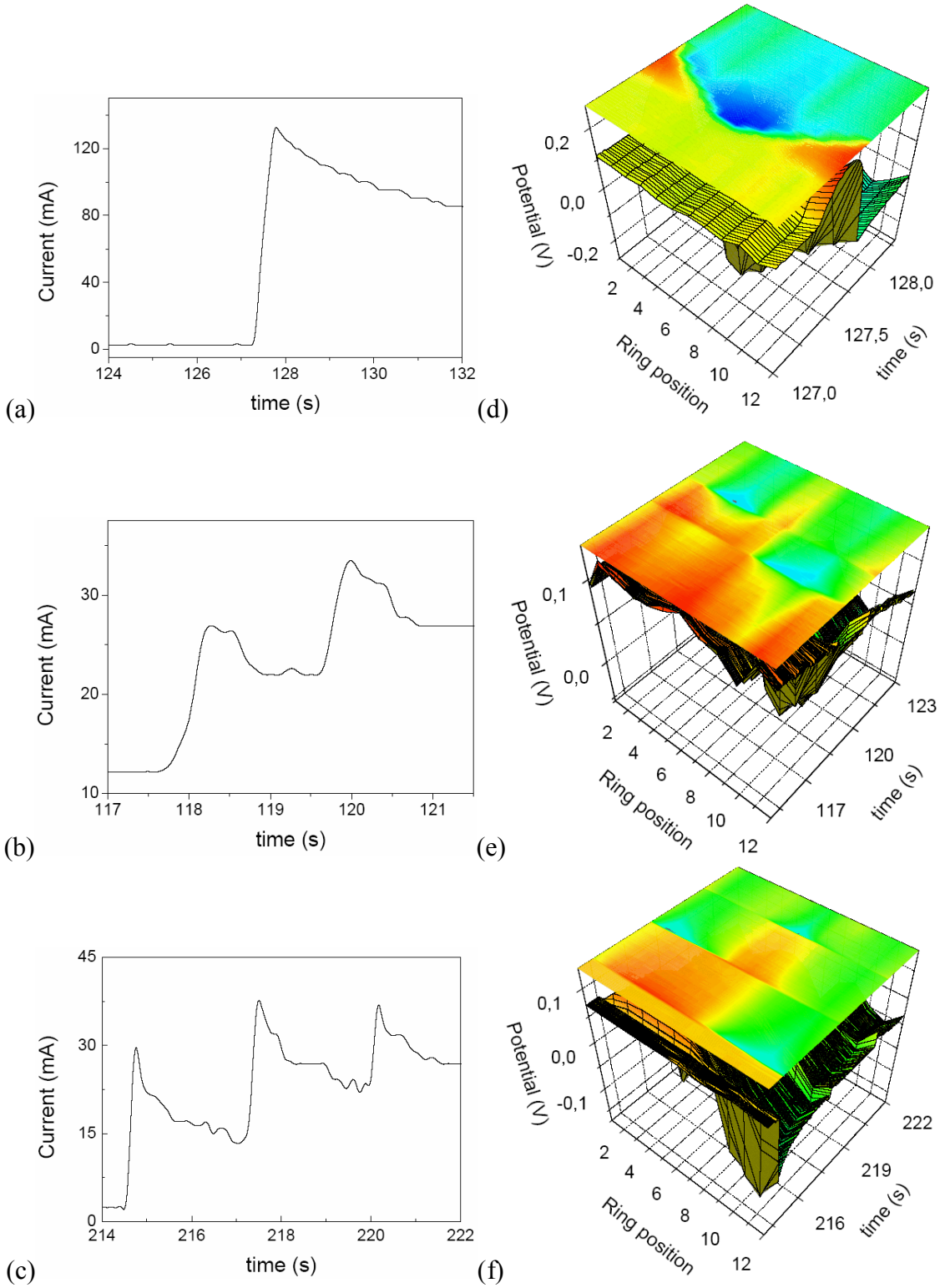

Figure 6.27. Time trace of current and spatiotemporal pattern of interfacial potential for the autonomous transition from passive to active state on a partially insulated ring electrode (β = 0). (a) one insulator, (b) two insulators, and (c) three insulators system.

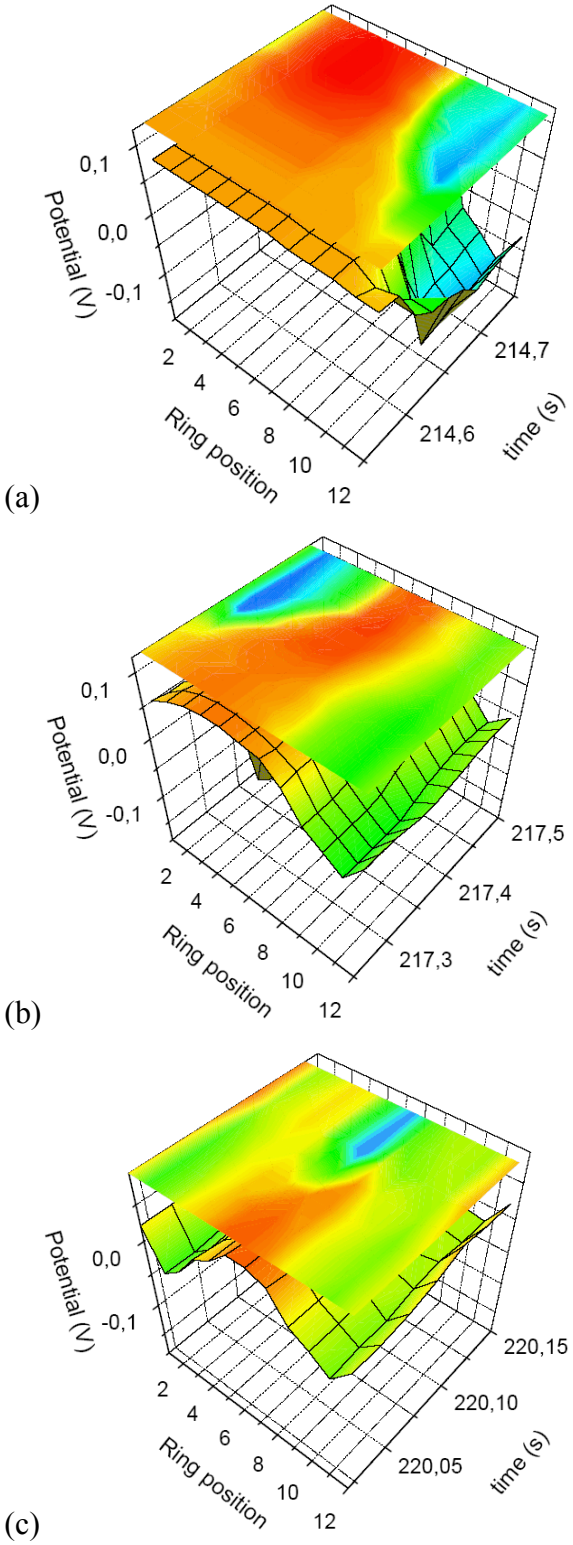

Figure 6.28. Enlargement of Figure 6.26(c). (a) an active front occurred first at position 11, (b) the next active front at position 2, (c) the last one at the position 7.

6.4 Discussion

The coupling function of the ring electrode system is well defined, which has symmetric electrode geometry [34]. With large distance of the reference electrode, all points along the ring are coupled positively with coupling strength decreasing with distance (positive coupling). However, a close reference electrode leads to a negative offset of the coupling function resulting in a negative nonlocal coupling along the ring electrode, *i.e.*, a positive short-range and negative long-range coupling. The negative nonlocal coupling has important consequences as to the dynamical behavior of the system. Two close points along the ring electrode tend to synchronize, while two distant points tend to be anticorrelated.

Coupling functions for complicated electrode geometries have been derived, for example disk and ribbon electrode, which assumed that each electrode is embedded in an insulating plane [34, 101]. In these cases, the most important difference compared to the ring electrode is the occurrence of edge effects. This effect manifests itself in a higher current density caused by a better current transport at the edges. Owing to these reasons, the local function diverges at the edges and the coupling function is much stronger at the edges than at other positions (remote migration coupling).

For a partially insulated ring electrode, one can assume that its coupling should be a mixture of the ring and ribbon system, because we get various dynamical patterns characteristic these systems. Firstly, there were patterns related with the ring system. During cyclic voltammetry, the pattern formation changed successively from standing waves to travelling pulses (Figure 6.5(a) and (b)). Furthermore, for close reference electrode, continuous travelling pulse (Figure 6.9), spontaneous pulse reversal in combination with mixed mode oscillations of the interfacial potential (Figure 6.10) were observed under constant potential conditions. Similar results have been investigated already in the ring system without insulation [71]. Secondly, there were patterns similar to a ribbon system. Under potentiostatic conditions, the two edges had higher interfacial potential compared with other positions at steady state in the active state (Figure 6.3), active fronts always started at maximum distance from the edges (Figure 6.27 and 6.28), and anti-phase edge oscillations of the interfacial potential were observed (Figure 6.6)

with close reference electrode. Such effects have also been observed on a ribbon [21, 106]. Thus, the partially insulated ring electrode exhibits edge effects like the ribbon while on the other parts it maintains to some extent the symmetry of the ring.

In addition, there were patterns on partially insulated rings the analogues of which had not been observed before on other electrodes. Thus there was evidence for period-doubled pulses (which repeat these shapes at every other rotation) on 1-, 2-, and 3-insulator ring electrodes (Figure 6.8, 6.18 and 6.24). For the 2- and 3-insulator systems in addition trapped patterns occurred, in which one subsystem between 2 insulators remains always passive (Figure 6.20 and 6.25).

An interesting effect on the partially insulated rings concerns the interaction of rotating pulses with the insulated areas. While very narrow insulators (≤ 3°) had virtually no effect, and too broad insulators (≥ 30°) caused propagation failure, for widths in between characteristic changes in the local pulse velocity were obtained; the pulses accelerated in the region close to the insulator (usually more in front than behind the insulator), then travelled continuously along the rest of the ring. This effect was clearest with 1 or 2 insulated areas, for the 3-insulator system the pulse seemed to interact with more than one insulator at the same time and no constant velocity could be obtained in between. The acceleration of pulses (*saltatory conduction*) can be rationalized in terms of the general theoretical framework of reaction-migration systems.

Charge balance at the electrode/electrolyte interface requires that the capacitive current i_c (given by the time derivative of the double layer potential u) and the faradaic (reaction) current i_r be balanced by the migration current i_m. The latter can be split into 2 terms; a local one depending on the local potential $u(x, t)$ and a global one given by an integral over the whole working electrode [34]

$$\frac{\partial u(x,t)}{\partial t} = -i_r + i_m = -i_r + \sigma h(x)(E - u(x,t)) + \sigma \int_{el} H_0(x,x')(u(x',t) - u(x,t))\, dx' \tag{6.1}$$

The conductivity σ of the electrolyte determines the coupling strength; the function *h(x)* takes into account that the local migration current depends on position (unless all point of the electrode are equivalent).

The integral term stems from the fact that electrical field effects are built up on a much faster time scale than the relevant chemical processes and spread very rapidly, they can be regarded as instantaneous, *i.e.*, every point *x* of the electrode communicates with every other one *x'* practically without delay through migration coupling. In general the coupling function $H(x, x')$ is locally high and steeply falls off with distance, a situation which could be reasonably well approximated with a (strictly local) diffusion term [106-109]. However, the coupling strength rises again near (and actually diverges at) a conductor/insulator interface due to the field distribution at the edge [34, 35]. Thus the uniform velocity far away from the edges results from the short-distance coupling, but a pulse approaching an insulated area will couple strongly to the parts adjacent to the insulator and activate them much more rapidly. This increased coupling strength at the conductor/insulator interface can account for the significant enhancement of the local velocity for small insulated areas. For too broad insulators, the drop in coupling with distance becomes dominant so that eventually the pulse cannot cross the gap any more.

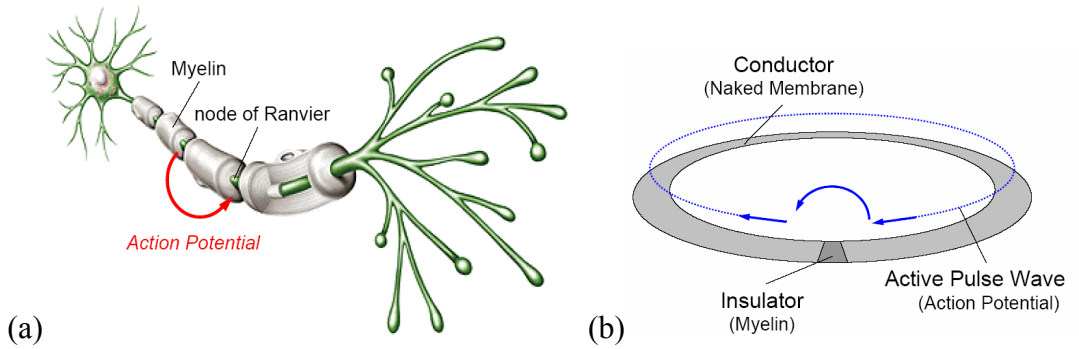

Figure 6.29. Saltatory conduction at (a) nerve cell and (b) ring electrode with insulator.

In nervous system, the propagation of an action potential along an unmyelinated axon is fundamentally the same as the electrochemical travelling pulse in the continuous excitable media. However, the presence of myelin changes the mode of transmission of the action potential. The action potential in myelinated axions can jump from node to node and speed up as a result of *saltatory conduction* instead of progressing along the region of axon covered by insulating myelin (Figure 6.29(a)). In the experiments described above we concentrated on the effect of insulated sections in order to show the unperturbed pulse and the effect of the insulator edges on its propagation velocity (Figure 6.29(b)).

The situation in nerve axons is somewhat more complicated [110-112]. The Ranvier nodes (1-2 mm in size) are typically separated by 1-2 mm of myelin-insulated axon. Since an excitation pulse can be around 30 mm long, it covers 15-20 Ranvier nodes at any given time. Still the propagation of the front end of the pulse is expected to be strongly accelerated by the enhanced coupling at the naked membrane/myelin interface. While an unmyelinated axon may be adequately described by a reaction-diffusion formalism (because the center of the axon acts like a zero-flux boundary which tends to localize the coupling), the cable model of saltatory conduction can account for the acceleration, essentially because the spatially averaged capacitance of the axon decreases so that the charge reversal takes less time compared to the unmyelinated case. Nevertheless the present results suggest an important contribution of the enhanced coupling at the conductor/insulator interface; consequently a refined theoretical approach for saltatory conductance ought to be based on reaction and migration with explicit consideration of edge effects.